AGU PUBLICATIONS

Geochemistry, Geophysics, Geosystems

RESEARCH ARTICLE
10.1002/2016GC006769

Incipient mantle plume evolution: Constraints from ancient landscapes buried beneath the North Sea

G. Stucky de Quay[1], G. G. Roberts[1], J. S. Watson[1], and C. A.-L. Jackson[1]

[1]Department of Earth Science and Engineering, Imperial College London, London, UK

Key Points:
- Sedimentary basins in the North Atlantic Ocean contain information about Paleogene vertical motions
- A buried terrestrial landscape in the Bressay region was uplifted in three stages between 58 and 55 Ma
- Rapid uplift and subsidence is best explained by transient asthenospheric thermal anomalies

Correspondence to:
G. Stucky de Quay,
g.stucky-de-quay14@ic.ac.uk

Citation:
Stucky de Quay, G., G. G. Roberts, J. S. Watson, and C. A.-L. Jackson (2017), Incipient mantle plume evolution: Constraints from ancient landscapes buried beneath the North Sea, *Geochem. Geophys. Geosyst.*, *18*, 973–993, doi:10.1002/2016GC006769.

Received 9 DEC 2016
Accepted 19 FEB 2017
Accepted article online 23 FEB 2017
Published online 16 MAR 2017

Abstract Geological observations that constrain the history of mantle convection are sparse despite its importance in determining vertical and horizontal plate motions, plate rheology, and magmatism. We use a suite of geological and geophysical observations from the northern North Sea to constrain evolution of the incipient Paleocene-Eocene Icelandic plume. Well data and a three-dimensional seismic survey are used to reconstruct a 58–55 Ma landscape now buried ~1.5 km beneath the seabed in the Bressay region. Geochemical analyses of cuttings from wells that intersect the landscape indicate the presence of angiosperm debris. These observations, combined with presence of coarse clastic material, interpreted beach ridges, and a large dendritic drainage network, indicate that this landscape formed subaerially. Longitudinal profiles of paleo-rivers were extracted and inverted for an uplift rate history, indicating three distinct phases of uplift and total cumulative uplift of ~350 m. Dinoflagellate cysts in the surrounding marine stratigraphy indicate that this terrestrial landscape formed in <3 Ma and was rapidly drowned. This uplift history is similar to that of a slightly older buried landscape in the Faeroe-Shetland basin ~400 km to the west. These records of vertical motion are consistent with pulses of anomalously hot asthenosphere spreading out from the incipient Icelandic plume. Using simple isostatic calculations, we estimate that the maximum thermal anomaly beneath Bressay was 50–100°C. Our observations suggest that a thermal anomaly departed the Icelandic plume around 57.4 ± 2.2 Ma at the latest and travelled with a velocity > ~150 km/Ma.

1. Introduction

Mantle convection and its interaction with the lithosphere are determinants of plate motion, lithospheric rheology, regional uplift and erosion, and magmatism [*Schubert et al*., 2001]. The generation of volcanism and rock uplift by mantle convection impacts the circulation and chemistry of the atmosphere and oceans. Epeirogenic uplift and erosion generated by mantle convection can determine sedimentary flux histories, which in turn control distribution and evolution of natural resources [*White and Lovell*, 1997; *Dam et al*., 1998; *Anell et al*., 2009; *Poore et al*., 2011]. Gravity data, seismic imaging, and the location and chemistry of magmatism provide information about the present-day state of the mantle [e.g., *McKenzie*, 2010; *Rickers et al*., 2013; *Matthews et al*., 2016]. For example, ocean-age depth measurements indicate that modern subplate support has amplitudes of ±1 km at wavelengths of 10^3 km. Positive anomalies of 1–2 km are present at wavelengths up to 2500 km close to the Icelandic, Hawaiian, Azorean, and Afar plumes [*Hoggard et al*., 2016]. A sparse set of uplift and denudation measurements of dynamically supported topography and the history of magmatism contain important clues about the temporal and spatial evolution of mantle convection [e.g., *White and McKenzie*, 1989; *Rudge et al*., 2008; *Hartley et al*., 2011; *Czarnota et al*., 2013; *Rowley et al*., 2013]. We focus on developing a suite of geologic observations that can be used to inform geodynamic modeling of the Earth's largest plume by buoyancy flux, located beneath Iceland, during its inception between ~62–55 Ma [*White and McKenzie*, 1995; *Parnell-Turner et al*., 2014].

1.1. Mantle Convection and the North Atlantic Ocean

The history of mantle convection is probably best understood beneath the North Atlantic Ocean and its surroundings where a combination of seismic, topographic, magmatic, thermochronological, and stratigraphic analyses constrain evolution of subplate support. Figure 1b shows regional dynamic topography calculated using long-wavelength (>800 km) free-air gravity anomalies extracted from the GOCE data set and admittance of 35 mGal km^{-1} [*Jones et al*., 2002a; *Förste et al*., 2014]. These calculations are broadly consistent with residual ocean-age depth measurements, which indicate that dynamically supported topography of

~2 km is centered on Iceland (Figure 1b) [*Hoggard et al*., 2016]. Positive anomalies extend east to the British Isles and Scandinavian Mountains and west to Greenland. *Rickers et al*. [2013]'s full-waveform S-velocity model has slow velocity perturbations, −2 to −9% relative to a modified version of the Preliminary Reference Earth Model (PREM), located directly beneath the plate below Iceland, along the Mid-Atlantic ridge, and in promontories that extend to the British Isles and Scandinavia [*Dziewonski and Anderson*, 1981]. These observations indicate that anomalously warm mantle extends >1000 km away from the Icelandic plume today. The location of thickest oceanic crust, gravity anomalies, shallow low-velocity anomalies in the upper mantle, earthquake hypocenters, intraplate volcanism, and high $^3He/^4He$ concentrations suggest the center of the plume is close to 65°N, 18°W today [*Óskarsson et al*., 1985; *Einarsson*, 1991; *Thorbergsson et al*., 1993; *Breddam et al*., 2000; *Darbyshire et al*., 2000; *Allen et al*., 2002]. The combination of receiver functions, wide-angle seismic data, ocean age-depth residuals, gravity data, and tomographic models indicate that the Icelandic plume supports up to 2 km of modern topography from Greenland to Norway (see Figure 1b) [*Darbyshire et al*., 2000; *Jones et al*., 2002a; *Rickers et al*., 2013; *Hoggard et al*., 2016]. Given that the Rayleigh number of Earth's mantle is 10^6-10^8, subplate support of topography is expected to be time-dependent [*White and McKenzie*, 1995]. This time-dependent behavior will punctuate histories of vertical motion generated by lithospheric shortening, stretching, and loading [*Sclater and Christie*, 1980; *White and McKenzie*, 1989; *Medvedev et al*., 2013; *Green et al*., 2013].

Seismic and multibeam imaging, gravity data, and geochemical modeling of dredged basalts from oceanic crust close to Iceland record 55–0 Ma of transient plume behavior [*Vogt*, 1971; *White et al*., 1995; *Jones et al*., 2002b; *Parkin et al*., 2007; *Parnell-Turner et al*., 2014]. These observations indicate that transient thermal anomalies occurred every 3–8 Ma and that buoyancy flux has varied through time. The transient behavior of the plume provides an explanation for punctuated Cenozoic uplift and subsidence of fringing sedimentary basins (e.g., northern North Sea), development of ephemeral landscapes, sedimentary drift and flux histories, magmatism, and oceanic circulation [e.g., *Jones and Milton*, 1994; *Liu and Galloway*, 1997; *Japsen and Chalmers*, 2000; *Underhill*, 2001; *Jones et al*., 2002a; *Mudge and Jones*, 2004; *Shaw-Champion et al*., 2008; *Anell et al*., 2009; *Poore et al*., 2009, 2011; *Hartley et al*., 2011].

The present-day distribution of Early Paleocene igneous rocks suggests that the Icelandic plume extended up to 1000 km away from its center in southeast Greenland, similar to its present-day extent [*White and McKenzie*, 1989]. Aluminum-in-olivine thermobarometry of a suite of ~61 Ma North Atlantic picrites indicates that the Paleocene Icelandic plume had an excess temperature up to 300°C [*Spice et al*., 2016]. Other Paleocene-Eocene plume centers have been proposed based on models of plate motion and continental stratigraphy, which place the plume in central Greenland or offshore southern Greenland (see Figure 1c) [*Lawver and Muller*, 1994; *Jones and White*, 2003]. In this study we use observations of uplift and subsidence of the Bressay region of the North Sea and the Judd region of the Faeroe-Shetland Basin to constrain the thermal and spatial evolution of the young Icelandic plume.

1.2. Manifestations of Plume Activity in the Northern North Sea

Figure 1d illustrates the present-day distribution of Paleocene and Lower Eocene sedimentary and igneous rock in the northern North Sea [*Mudge*, 2015]. The Faeroe Platform is covered by Paleocene lavas. The Bressay region, which sits on the eastern edge of the deltaic Dornoch Formation, is flanked by the East Shetland Platform and the Viking Graben. The West and East Shetland platforms and the Norwegian Platform are devoid of Paleocene or Eocene sedimentary rock [*Mudge and Bujak*, 2001].

The Faeroe-Shetland, Moray Firth, and North Sea basins contain coarse Paleocene-Eocene terrestrial sandstones sandwiched between marine mudstones. These observations indicate that these regions experienced a short-lived (<3 Ma) history of marine-terrestrial-marine conditions close to the Paleocene-Eocene boundary [*Mudge and Bujak*, 2001; *Underhill*, 2001; *Mudge and Jones*, 2004; *Mackay et al*., 2005; *Shaw-Champion et al*., 2008]. In the Judd region of the Faeroe-Shetland Basin, north of Scotland, an erosional unconformity has been mapped at the base of the coarse sandstone Flett Formation (Figure 2). Depth conversion and decompaction of infilling stratigraphy and recorded lignite suggest that the unconformity was created by erosion of a terrestrial landscape with at least 900 m of relief [*Shaw-Champion et al*., 2008; *Hartley et al*., 2011]. Dinoflagellate and pollen chronostratigraphy indicate that this landscape formed close to 55 Ma. Longitudinal profiles extracted from this surface have almost 1 km of relief and contain three large (>100 m of relief) knickzones [*Hartley et al*., 2011].

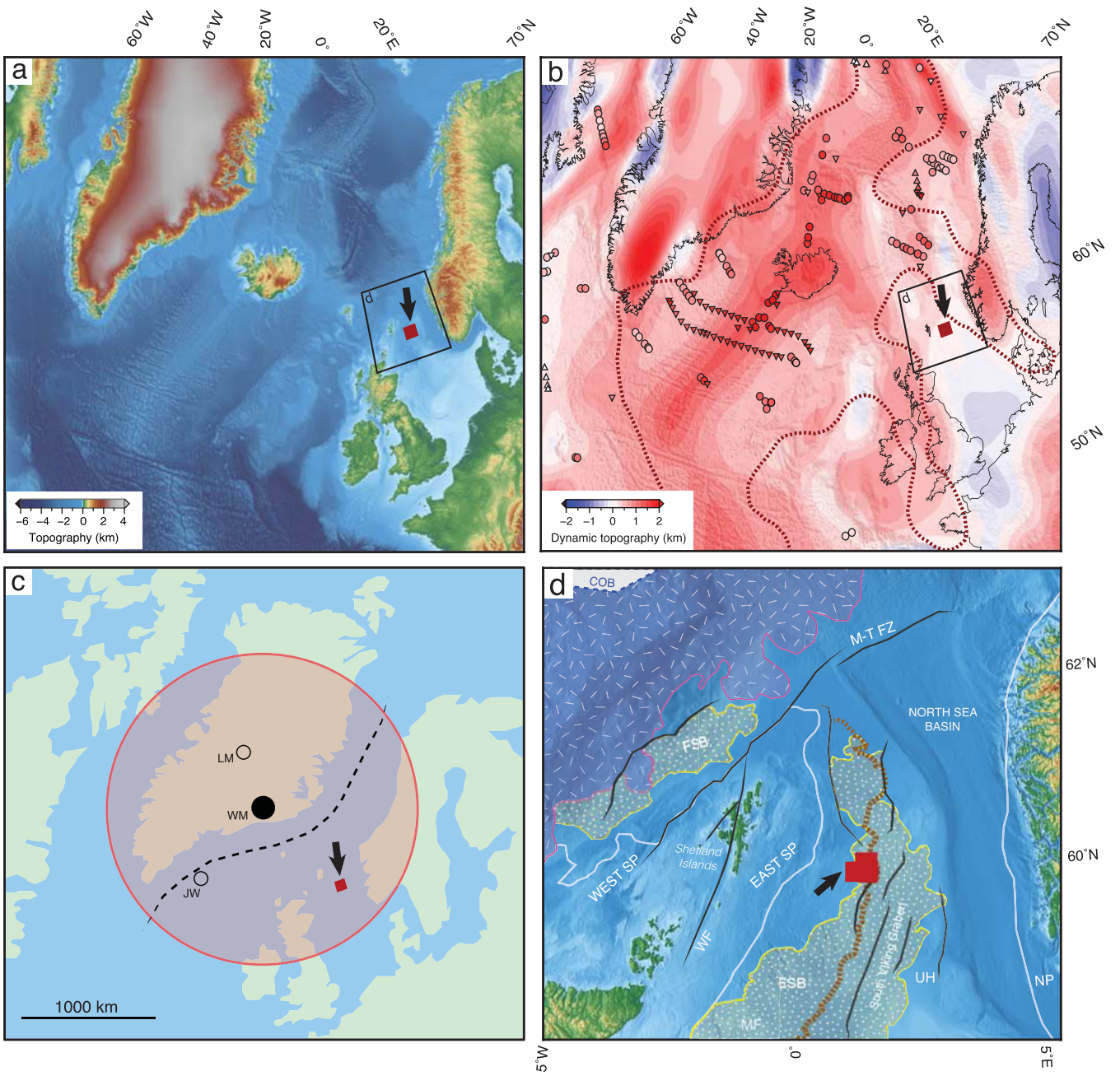

Figure 1. (a) North Atlantic Ocean topography and location of Bressay region (red square) [*Smith and Sandwell*, 1997]. (b) Dynamic support of the North Atlantic Ocean calculated using long-wavelength (>800 km) free-air gravity anomalies (obtained from GOCE [*Förste et al.*, 2014]) and a constant admittance of Z = 35 mGal km^{-1} appropriate for subaqueous regions [*Jones et al.*, 2002a]. Dashed red line encompasses S-velocity perturbation <−2% between 100 and 200 km depth [*Rickers et al.*, 2013]. Circles = residual topography from age-depth measurements; upward/downward pointing triangles = minimum/maximum values [*Hoggard et al.*, 2016]. (c) Simplified reconstruction of the North Atlantic Ocean at 55 Ma. Black circle labeled WM = center of *White and McKenzie* [1989] Icelandic plume; open circles labeled LM/JW for *Lawver and Muller* [1994] and *Jones and White* [2003] plume centers; red transparent circle = approximate extent of idealized axisymmetric plume; dashed black line = location of continental breakup [*White and McKenzie*, 1989]. (d) Bressay region and its surroundings. Red box = 3-D seismic data set. Yellow stippled areas = slope and basin sands; pink edged polygon = Paleocene lavas; orange dashed line = eastern limit of the Dornoch delta; black lines = faults; COB = continent-ocean boundary, ESB = East Shetland Basin, FSB = Faeroe-Shetland Basin, SP = Shetland Platform, M-T FZ = Møre-Trøndelag Fault Zone, NP = Norwegian Platform, WF = Walls Fault, UH = Utsira High [*Mudge*, 2015].

A slightly younger and lower relief (<300 m) landscape was mapped in the Bressay region using seismic and well data by *Underhill* [2001], in the East Shetland Platform of the northern North Sea. Buried extensional faults and backstripped well data indicate that the East Shetland Platform was stretched by a factor $\beta = 1.3 \pm 0.04$ from the Late Jurassic for ~60 Ma [*White*, 1990; *Underhill*, 2001]. It currently sits on the eastern fringe of the Icelandic plume (Figure 1b).

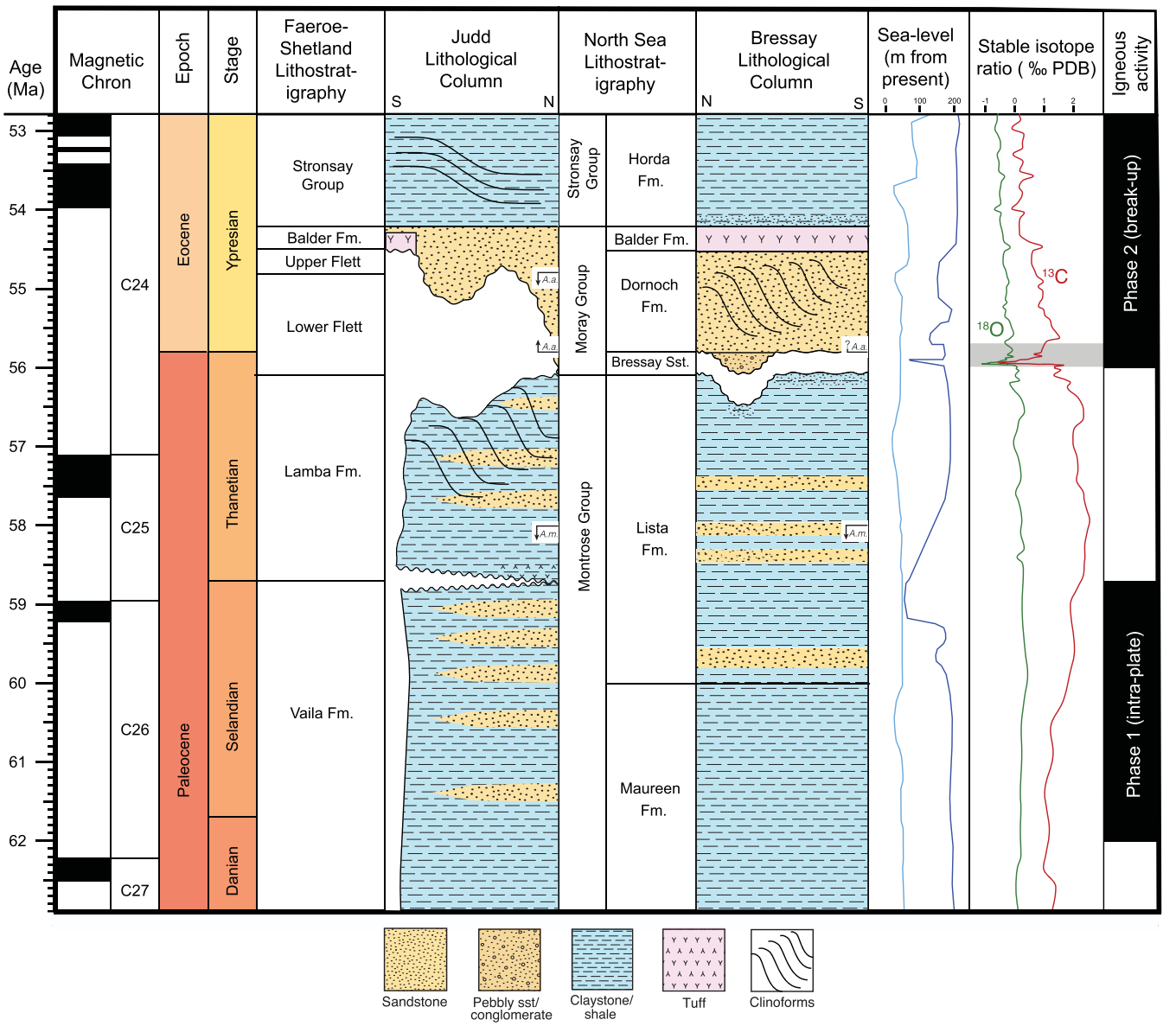

Figure 2. Paleocene-Eocene chronostratigraphy of Judd [*Shaw-Champion et al*., 2008] and Bressay regions. Bressay stratigraphy is dated using dinoflagellate cyst records (see Appendix Table A1). Lithostratigraphy nomenclature is based on *Knox and Holloway* [1992]. Ages for dinocysts *Apectodinium augustum* (*A.a.*) and *Alisocysta margarita* (*A.m.*) are from *Luterbacher et al*. [2004]. Light and dark blue sea level curves are from *Miller et al*. [2005] and *Haq et al*. [1988], respectively. Isotope curves are obtained from *Cramer et al*. [2009]. Gray band = Paleocene-Eocene Thermal Maximum (PETM), ~170 ka [*Röhl et al*., 2007]. Igneous activity is summarized from *Saunders et al*. [1997].

The rapidity and amplitude of the Paleocene-Eocene vertical motions of these regions suggest that glacio-eustasy, shortening (and erosion), or underplating are unlikely to be responsible for generating observed uplift and subsidence. Instead, *Shaw-Champion et al*. [2008] suggested that they are a manifestation of the incipient Icelandic plume. Histories of uplift extracted from these landscapes are the crucial observations used to constrain velocities and temperatures of the incipient Icelandic plume [e.g., *Rudge et al*., 2008; *Hartley et al*., 2011]. Kinematic models of asthenospheric flow combined with simple isostatic calculations suggest that the Paleogene vertical motions of Judd were produced by three thermal anomalies passing beneath the plate with excess temperatures up to 130°C [*Rudge et al*., 2008; *Hartley et al*., 2011].

Until now the shape and age of the Bressay erosional surface has been poorly constrained, which has made it difficult to test these models. Fortunately, 900 km^2 of new three-dimensional seismic data and seven commercial wells are available for mapping courtesy of PGS and Statoil (Figure 3). The wells have excellent

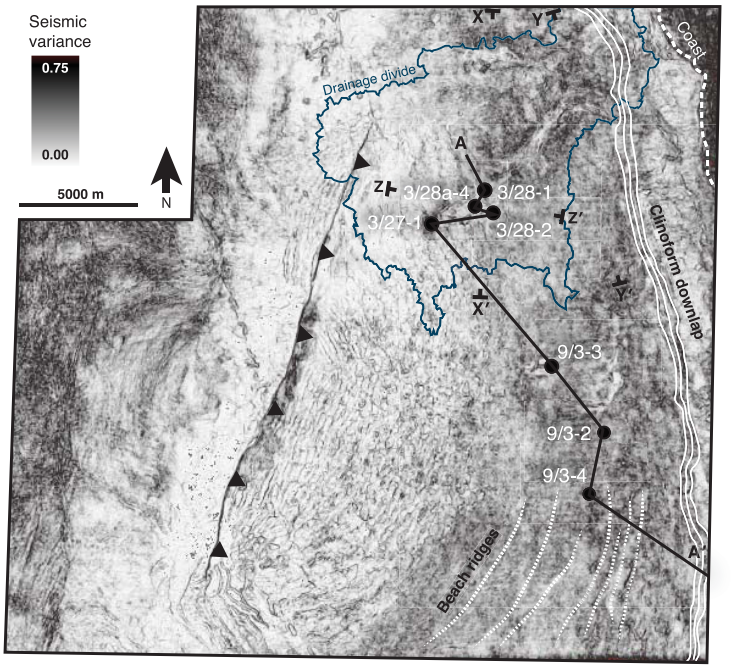

Figure 3. Depth-slice of seismic variance (trace-to-trace variability) at 1400 ms from 3-D seismic volume. Black circles = wells used in this study. Regional cross section along wells = A–A′ (see Figures 4 and 6). Cross sections along channel = X–X′, Y–Y′, and Z–Z′ (see Figure 7).

biostratigraphic and checkshot data. We use these data to map and date Bressay's Paleogene erosional surface and combine results with those from Judd to estimate the history of vertical motions of the northern North Sea as the Icelandic plume impinged upon the lithosphere 62–55 Ma. These observations are used to estimate the temperature and velocity of the Paleocene mantle beneath the incipient North Atlantic Ocean.

2. Data Processing and Methods

2.1. Well Data

We summarize the lithostratigraphy of the Bressay region based on well reports and published work. The locations of the exploration wells in the study area are shown in Figure 3: 3/27-1, 3/28-1, 3/28-2, 3/28a-4, 9/3-2, 9/3-3, and 9/3-4. Gamma-ray data, stratigraphic charts, and biostratigraphic records have been combined to generate a stratigraphic framework for the upper 1.5 km of the Bressay region, which is summarized using the nomenclature of *Knox and Holloway* [1992] and *Underhill* [2001] (Figures 2 and 4).

At the bottom of the section of interest, the boundary between the Chalk Group and the overlying Paleocene Montrose Group records the onset of Cenozoic clastic deposition in the basin. The base of the Montrose Group has successions of interbedded chalk and local sandstone. The group is subdivided into the Maureen and Lista Formations. The Lista Formation contains sand accumulations separated by pelagic muds, and the Maureen Formation is generally indicated by a downward change into more calcareous sandstone, reworked limestone, or marl [*Knox and Holloway*, 1992].

The Lista Formation has a sharp contact with the overlying Moray Group. These units are conformable in wells 9/3-2, 9/3-3, and 9/3-4 (see red boundary in Figure 4). In wells 3/27-1, 3/28-1, 3/28-2, and 3/28a-4 the marine mudstones of the Lista Formation are unconformably in contact with overlying coarse-grained, well-rounded, poorly sorted sandstone and pebbly sandstone containing wood fragments (see Figure 5b). Heavily oil-stained mudstones occur intermittently throughout this section, which contains the Dornoch Formation and the Bressay Sandstone (Figure 5c). *Underhill* [2001] suggested that the pebbly sandstone facies of the Bressay Sandstone are the basal fluvial infill of incised channels. The Bressay Sandstone's stratigraphic position relative to the deltaic Dornoch Formation is a crucial constraint on the history of Paleocene-Eocene vertical motions and is the focus of this study. We examine the age of this unconformity in more detail in section 2.3.

The Dornoch Formation in wells 9/3-2, 9/3-3, and 9/3-4 is conglomeratic and contains traces of terrigenous plants and pollens. The uppermost unit of the Moray Group is the Balder Formation. It consists of carbonaceous, tuffaceous mudstones, with tuff-rich layers at its base. The formation is roughly uniform in thickness throughout the study area (~30 m). The upward gradation from tuff into mudstones most likely reflects a rise in sea level as well as a decrease in pyroclastic activity [*Knox and Morton*, 1988].

The Stronsay Group overlies the Balder Formation and consists of marine mudstones and subordinate sandstones. This stratigraphy suggests a rapid return to marine conditions by ~54.5 Ma [*Knox and Holloway*,

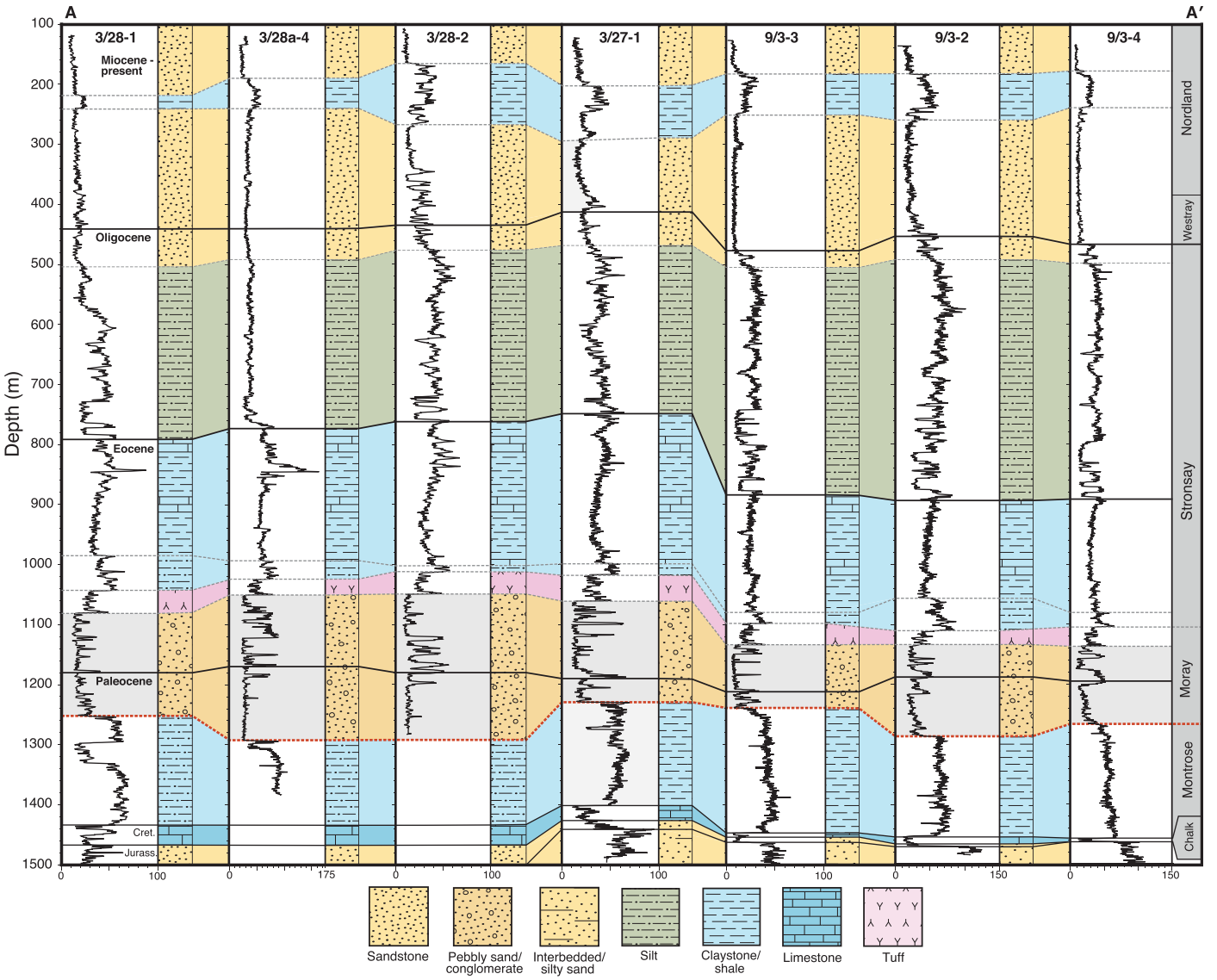

Figure 4. Gamma-ray data for seven wells shown along A–A′ line in Figure 3. Dashed gray lines = lithological boundaries; solid black lines = age boundaries; red line = unconformity.

1992]. The Stronsay Group extends into the earliest Eocene and is overlain by the Westray Group, which is formed of early Oligocene to mid-Miocene marine mudstones. This stratigraphic sequence is overlain by the Nordland Group, consisting of silty mudstones and siltstones which were most likely deposited in a shallow marine setting [*Andrews et al.*, 1990].

To determine the history of vertical motions of Bressay as the Icelandic plume began to grow, we need to accurately determine the depositional environment and age of the Bressay Sandstone.

2.2. Organic Geochemistry

To determine the origin of the oldest sedimentary rock (Dornoch Formation/Bressay Sandstone) that infills the unconformity, we measured the organic content of core cuttings from well 3/28a-4 at a depth of 1298 ± 10 m.

Samples were powdered in a pestle and mortar and then solvent extracted (ca. 1.5 g). Internal standards (squalane and *p*-terphenyl) were added to each sample prior to extraction. The powdered samples were placed in test tubes and 4 ml of dichloromethane (DCM):methanol (93:7 v/v) added. The mixture was then sonicated for 3 min, centrifuged, and the supernatant was removed; the extraction process was repeated

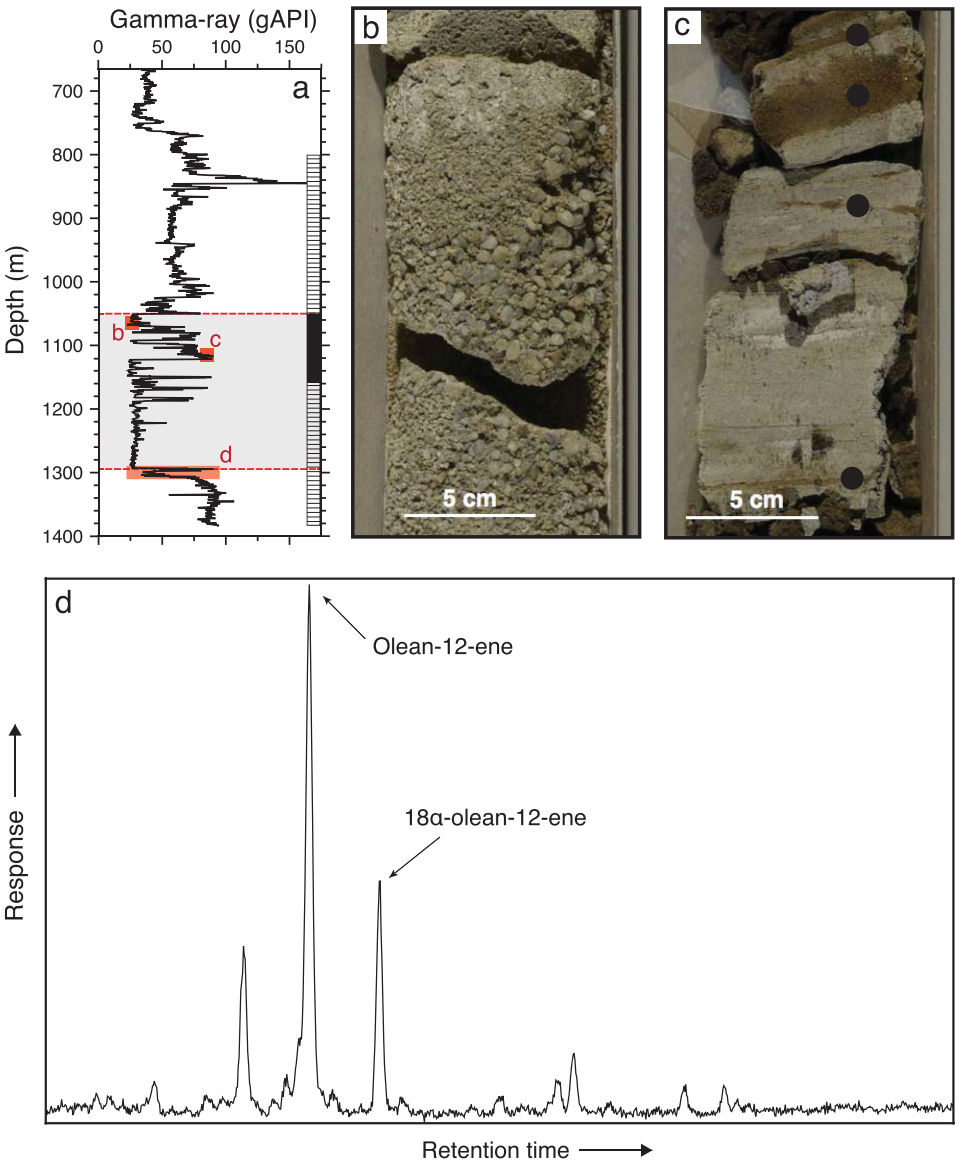

Figure 5. (a) Gamma ray data for well 3/28a-4. Hachures = cuttings; solid black rectangle = core. Gray band = extent of channel fill (i.e., Bressay Sandstone). Pink squares = locations of core shown in Figures 5b and 5c. Pink rectangle = location of cuttings used for analysis shown in Figure 5d. (b) Core from 1051 m depth. Note coarse sands/pebbles and gamma-ray <50 gAPI in Figure 5a. (c) Core from 1120 m depth. Note shaly facies and gamma-ray >75 gAPI. Black circles = oil staining. Photographs from Figures 5b and 5c were obtained from British Geological Survey offshore well drillcore database (© NERC). (d) GC-MS (partial mass chromatogram *m/z* 218) of hydrocarbon fraction of sample at 1298 m depth displaying two prominent oleanene peaks.

three times. After extraction, activated copper turnings were added into each sample to remove elemental sulfur and then the combined supernatants were taken to dryness under a stream of dry nitrogen in a preweighed vial. The concentrated extracts were fractionated by column chromatography using activated alumina powder in which the total hydrocarbon fraction was eluted using hexane and DCM:hexane (1:1 v/v). The hydrocarbon fraction was concentrated (ca. <0.2 ml) using dry nitrogen prior to analysis by gas chromatography-mass spectrometry (GC-MS).

GC-MS analysis was carried out on aliphatic and aromatic fractions of the samples using an Agilent Technologies 7890A gas chromatograph (GC) coupled to a 5975C mass spectrometer. The GC injector was operated in a splitless mode (1 μl) with a column flow rate of 1.1 ml min^{-1}. A J&W scientific DB-5MSUI capillary column (30 m, 250 μm i.d., 0.25 μm film thickness) was used for separation and helium employed as a carrier

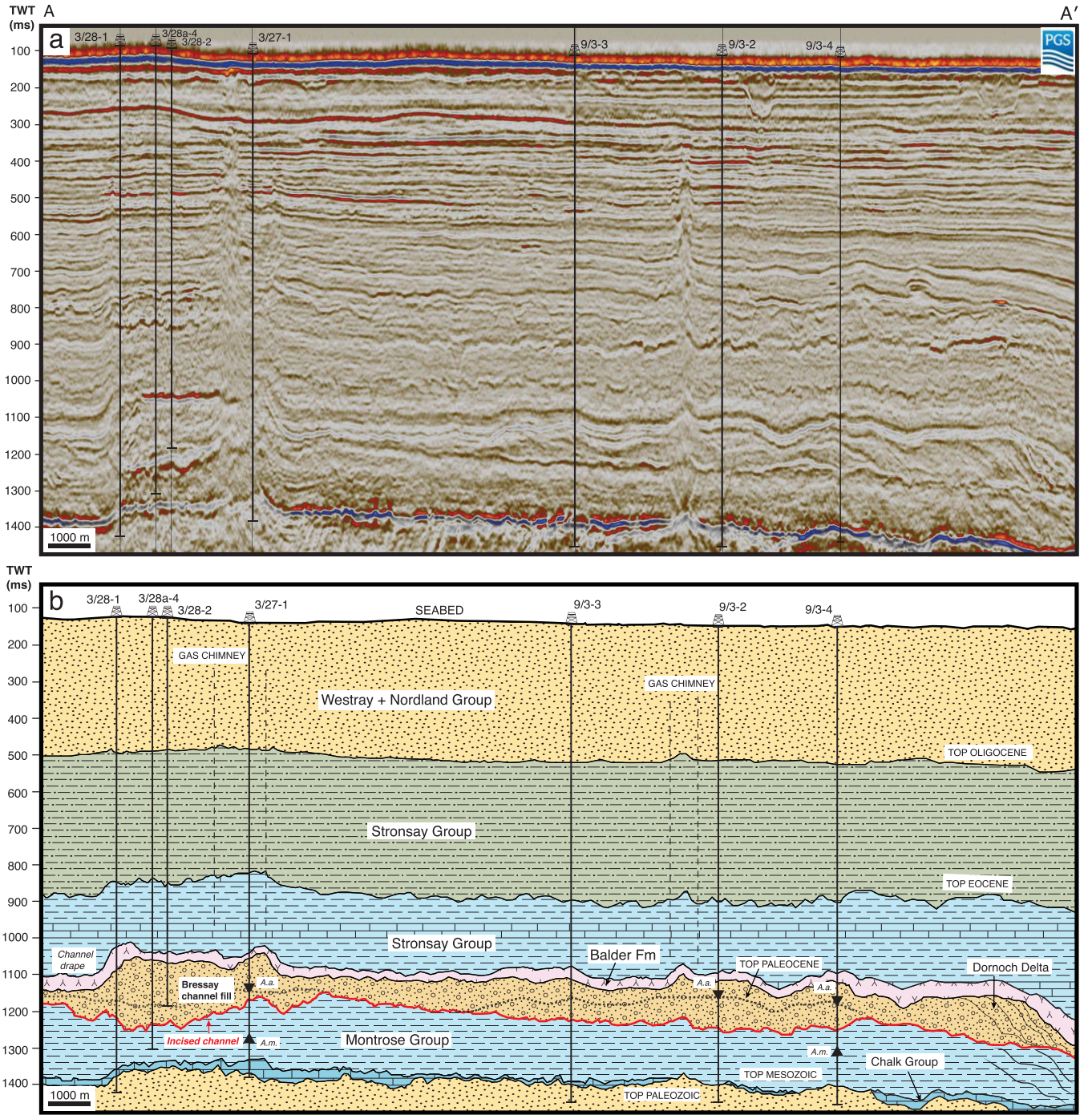

Figure 6. (a) Vertical seismic slice along A–A′ trace from Figure 3. TWT = two-way time. (b) Interpreted stratigraphy. Red line = incised surface; solid vertical lines = well paths; dashed vertical lines = gas chimneys; dotted line = Paleocene-Eocene boundary. Lithological key is shown in Figure 4. Up/down pointing black arrows = location of dinocysts *A.m./A.a.* that constrain the age of the unconformity.

gas. The GC oven temperature was initially held at 40°C for 2 min, and then raised to a 310°C at a rate of 5°C min^{-1} where it was held for 14 min. Mass spectra were acquired in electron impact mode (70 eV) in the scan range of 50–500 amu and also in selective ion monitoring (*m/z* 177, 191, 205, 217, 218).

Two oleanene isomers (olean-12-ene and 18α-olean-12-ene) were identified in the extracts. The partial mass fragmentogram (*m/z* 218) of the hydrocarbon fraction of the extract that contains the oleanenes is shown in Figure 5d. Oleanenes in oils have been linked to angiosperm debris in Cenozoic or Cretaceous source

rocks and to deltaic depositional settings [*Eneogwe et al*., 2002]. The occurrence of the two oleanene isomers in this sample likely favors a terrestrial origin for the organic matter, deposited either in a lacustrine, fluvial, estuarine, or deltaic/shallow marine environment [*Adedosu et al*., 2010]. These observations are consistent with well logs that document the presence of spores, pollens, wood, coals, and lignites within the sandstone deposited directly above the Paleocene-Eocene unconformity. With the samples available we cannot rule out reworking of more proximal material. However, the presence of different types of organic matter and an upward coarsening of clastic material observed in most wells (e.g., Figure 4) suggests that the unconformity developed in a subaerial environment.

2.3. Biostratigraphic Dating

Three of the wells in our study area, 3/27-1, 9/3-2, and 9/3-4, contain biostratigraphic records and >150 distinct dinoflagellate cysts (dinocysts) species are observed. Palynomorphs, including cysts of marine planktonic dinoflagellates, and spores and pollens of terrestrial plants, are abundant. Of these, dinocysts are the most suitable for dating the Paleocene-Eocene boundary due to their abundance and high temporal resolution [*Mudge and Bujak*, 1996]. Dinocyst appearances from 14 key specimens and associated ages are provided in Appendix (Table A1).

Nine Eocene biomarkers are located within the Stronsay, Balder, and Dornoch Formations. Six of these dinocysts have their first appearance at the Paleocene-Eocene boundary and occur in the uppermost Bressay Sandstone. Dinocysts *Glaphyrocysta ordinata* (*G.o*), *Palaeoperidinium pyrophorum* (*P.p*), and *Ceratiopsis speciosa* (*C.s*.) straddle the Paleocene-Eocene boundary. These 12 markers are dated using ages provided in *Williams and Bujak* [1989].

However, the two biomarkers most effective for constraining the age of the Paleocene-Eocene Bressay unconformity are *Apectodinium augustum* (*A.a*.) and *Alisocysta margarita* (*A.m*.). *A.a*. occurs in the Bressay Sandstone, above the unconformity, whereas *A.m*. is found in the Lista Formation below the unconformity (see Figures 2 and 6). The age ranges used in this study are based on those presented by *Luterbacher et al*. [2004], although other ages for these two dinocysts have been proposed by *Mudge and Bujak* [2001] and *Vandenberghe et al*. [2012], which are slightly younger and older, respectively. Using *Luterbacher et al*. [2004]'s ages, *A.a*. has its first appearance at 55.8 Ma and last appearance at 54.8 Ma. This is consistent with an Early Eocene age for *A.a*. in the northern North Sea and is supported by several authors [e.g., *Mudge and Copestake*, 1992; *Gradstein et al*., 1992; *Mudge and Bujak*, 1994; *Neal*, 1996; *Thomas*, 1996]. *A.m*. occurrences are 59.2–58.0 Ma. The unconformity must have developed after the last appearance of *A.m*. (58.0 Ma) and before the last appearance of *A.a* (54.8 Ma). Combined with evidence for terrestrial organic matter, this observation suggests the unconformity developed subaerially around 58–55 Ma.

2.4. Reflection Seismic Data

Having used well data to establish the presence of a ~58–55 Ma unconformity, we now incorporate seismic reflection data and well correlations to map the geometry of the erosional surface across the Bressay region. The seismic survey is centered at ~1°E, 60°N and includes 2434 inlines and 2248 cross lines covering ~30× 30 km (Figure 3). The survey extends to ~5 km beneath the seabed. Note that wells penetrate only the shallowest 1.5 km (Cretaceous and younger stratigraphy). Figure 3 shows a horizontal slice through seismic variance (trace-to-trace variability) at a depth of 1400 ms (~1.3 km) in two-way time (TWT), which intersects the contact between the Paleocene-Eocene unconformity.

Figure 6 shows an interpreted cross section along the line A–A′ shown in Figure 3. In some places gas chimneys make interpretation challenging and velocity pull-up is observed in the chalk unit beneath them. Stratigraphy is generally subparallel, which indicates that Cenozoic horizontal shortening is modest. The unconformity is highlighted in red and incision is most pronounced at 1200 ms depth toward the north. The unconformity sits atop the Montrose Group, which contains dipping impedance contrasts to the southeast which we interpret as clinoforms. The deltaic Dornoch Formation with clinoformal geometries sits atop the unconformity (Figure 6). The black arrows show the first/last occurrence of *A.a*. and the last occurrence of *A.m*. in wells 3/27-1, 9/3-2, and 9/3-4. The V-shaped features, which have high variance at contacts with underlying stratigraphy, are most likely fluvial channels. Patches of high variance in Figure 3 outline a dendritic pattern in the northeast that is in the same location as the drainage network mapped by *Underhill* [2001].

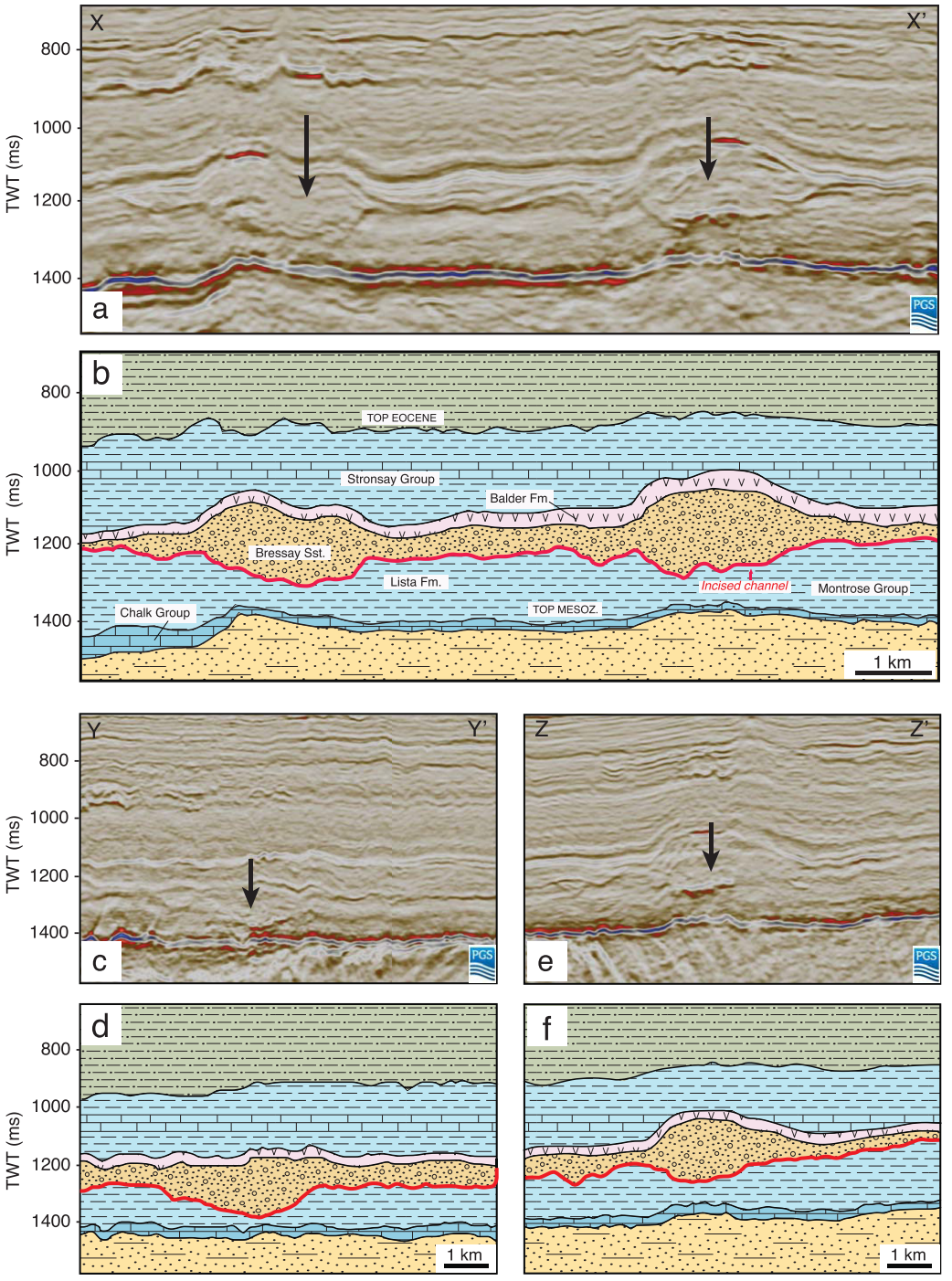

Figure 7. (a) Cross section X–X′ of seismic data shown in Figure 3; black arrows indicate channels. (b) Interpreted seismic and well data. Incised surface is shown by red line. (c, d) Cross-section Y–Y′. (e, f) Cross-section Z–Z′.

Figure 7 shows cross sections through tributaries of the drainage network. The Bressay Sandstone has a maximum thickness of ~250 ms in these channels and incises into the Lista Formation. Cross sections X–X′ and Z–Z′ show steep and narrow valleys. Cross section Y–Y′ is located in the far northeastern part of the survey and shows that the valley here is wider and its walls have lower slopes. The Balder Formation drapes the Bressay Sandstone and Dornoch Formation and mirrors the relief of the underlying unconformity (e.g., Figure 7). This relief is probably caused by differential compaction due to the sandy fill of incised valleys compacting less than adjacent mudstones.

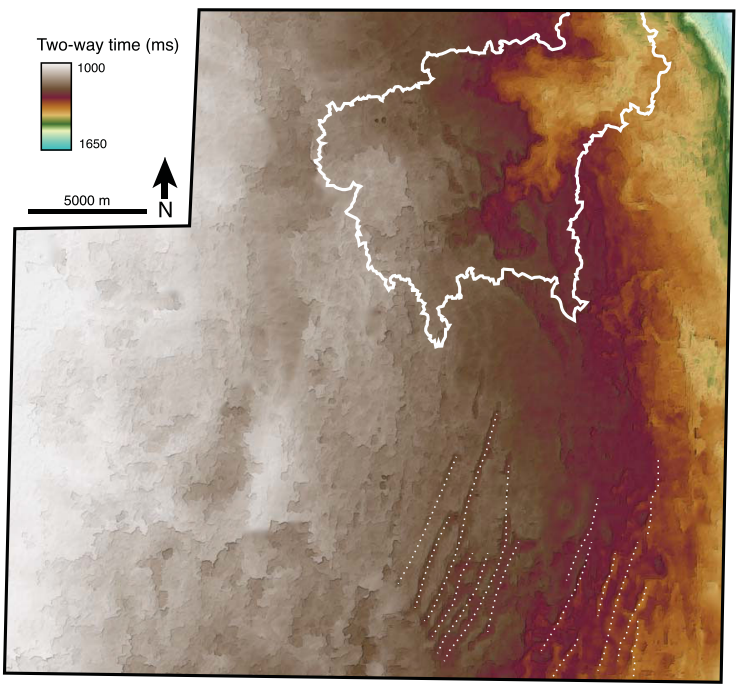

Figure 8. Extracted Bressay channel surface in two-way time. White outline = extent of drainage basin. White dotted lines = beach ridges and troughs.

The unconformity was mapped across the study area using every inline and cross line (i.e., no autotracking). The resultant landscape is shown in Figure 8. It has a resolution of ~12 × 12 m. Two large catchments drain toward the east. The valley located toward the northeast of the surface has a relief of ~250 ms. The mapped drainage network has a dendritic pattern upstream and a widening central valley downstream.

Our observations differ from *Underhill* [2001]'s work in three subtle but important ways. First, we show that the Paleocene-Eocene unconformity does not sit atop the Dornoch Formation, rather that the Dornoch Formation was deposited on top of the unconformity. Second, although mapped as a dendritic drainage network by *Underhill* [2001], remapping of the southeast quadrant indicates that these features tend to be unconnected and subparallel to the paleo-coastline. They are more likely beach ridges [e.g., *Jackson et al.*, 2010]. Finally, remapping the top of the Dornoch Formation indicates that it possesses no coherent or connected drainage network. These observations combined with dinocyst records indicate that the Paleocene-Eocene unconformity is 0.1–1.3 Ma older than suggested by *Underhill* [2001] and *Rudge et al.* [2008] (54.7–54.5 Ma). To examine the geomorphology of the Bressay landscape as it formed, we depth-converted and decompacted the rock that infills this unconformity for its thickness at time of deposition. Drainage patterns were then extracted from this surface.

2.5. Depth Conversion

To convert the landscape from two-way travel time, t, to depth, z, we use check-shot measurements. Five of the seven wells in this study have check-shot data, and all are almost vertical such that measured depth is approximately true vertical depth. Observed time-depth pairs for five wells are shown as gray lines in Figure 9a. Time-depth data for wells intersecting channels and gas columns (3/27-1 and 3/28a-4) are similar to those outside channels (9/3-2, 9/3-3, and 9/3-4) (Figures 6 and 9a). In addition, seismic data indicates that the Paleogene and younger stratigraphy dips shallowly. Both these observations suggest that a one-dimensional velocity model is acceptable. We fit a quadratic function to observed time-depth pairs, such that $z=0.0164t^2+0.8719t$ (red line in Figure 9a, $r^2=0.99$). A 1σ deviation is used to estimate uncertainty in the time to depth conversion.

2.6. Decompaction

Once the mapped landscape is converted into depth, we can then correct for compaction from loading to recover the relief of the landscape. We quantify the amount of compaction using a well-known relationship between porosity, ϕ, and depth, z,

$$\phi(z)=\phi_\circ \exp\left(\frac{-z}{\lambda}\right), \tag{1}$$

where $\phi_\circ$ is initial porosity and λ is compaction wavelength. We use an empirical relationship to constrain $\phi_\circ$ and λ as a function of depth and velocity,

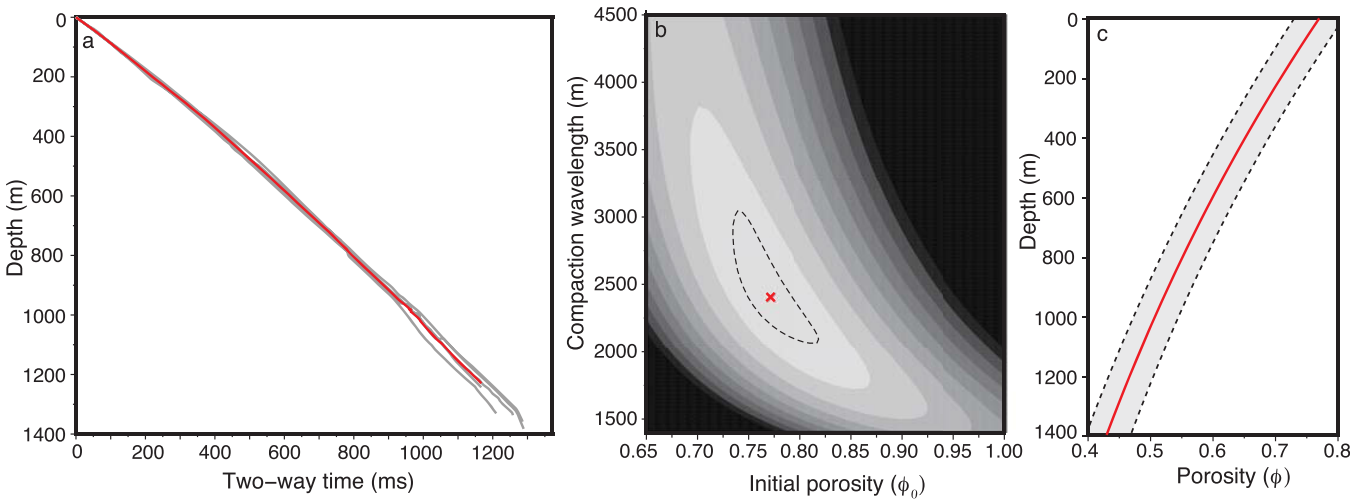

Figure 9. (a) Check-shot time-depth data for five wells in Bressay region, 3/27-1, 3/28a-4, 9/3-2, 9/3-3, and 9/3-4, are shown in gray; red line = mean values. (b) Misfit between observed and theoretical time-depth pairs as a function of compaction wavelength (λ) and initial porosity ($\phi_\circ$). Red cross = lowest misfit ($\phi_\circ = 0.77$, $\lambda = 2400$ m); dashed line = error envelope of ±5%. (c) Porosity as function of depth for the Bressay region using best fitting decompaction parameters. Dashed line = ±5% error.

$$\frac{t}{2} = \frac{z}{v_{sg}} + \phi_\circ \lambda \left(\frac{1}{v_w} - \frac{1}{v_{sg}} \right) \left\{ 1 - \exp\left(\frac{-z}{\lambda} \right) \right\}, \tag{2}$$

where constants v_{sg} and v_w are the interval pore fluid sonic velocity (1.5 km s^{-1}) and the solid grain velocity (5.5 km s^{-1} for clastic sediments), respectively [*Wyllie et al.*, 1956; *Sclater and Christie*, 1980; *Christensen*, 1982; *Czarnota et al.*, 2013]. We compare observed and theoretical time-depth values for different combinations of $\phi_\circ$ and λ. Misfit is lowest when $\phi_\circ = 0.77$ and $\lambda = 2.4$ km (rms misfit = 0.37; Figure 9b). These values can then be inserted into equation (1) to calculate porosity as a function of depth (Figure 9c). We decompacted the sedimentary rock between the eroded landscape and a continuous curvature summit envelope constrained by drainage divide loci [*Wessel and Smith*, 1990]. The volume between these surfaces is a minimum estimate of the amount of material eroded from the Bressay landscape. To decompact, the solid fraction is conserved such that,

$$\int_{z_1}^{z_2} 1 - \phi(z) \mathrm{d}z = \int_{\circ}^{z_3} 1 - \phi(z) \mathrm{d}z, \tag{3}$$

where $z_2 - z_1$ is the compacted thickness of the layer and z_3 is the depositional thickness of the layer. Substituting equation (1) in and integrating yields,

$$z_3 = z_2 - z_1 - \phi_\circ \lambda [\exp(-z_1/\lambda) - \exp(-z_2/\lambda) + \exp(-z_3/\lambda) - 1]. \tag{4}$$

Equation (4) can be solved by Newton-Raphson iteration for the depositional thickness of the infill of the Bressay landscape, z_3. z_1 and z_2 are the respective depths of the summit envelope (i.e., thickness of the overburden) and erosional surface. Following depth-conversion and decompaction, the reconstructed landscape can be used to extract drainage patterns (see Figure 10a).

2.7. Drainage Extraction

To extract a drainage network, Esri flow routing algorithms were applied to the digital elevation model (Figure 10b). First, flow direction is calculated using the steepest descent from each cell in the digital elevation model [*Tarboton*, 1997]. Second, flow accumulation to each cell is measured. Finally, flow lengths are calculated and drainage patterns extracted. The drainage inventory includes 87 rivers. Their longitudinal profiles are shown in Figure 11a. The rivers have up to 350 m of relief and contain knickzones with tens to hundreds of meters of relief, which is much greater than seismic resolution (few meters). The lithological and structural characteristics of river substrate and infilling stratigraphy can be explored using seismic data extracted along rivers. A seismic profile, extracted along the river shown in blue in Figure 11a, is shown in Figures 11b and 11c. There is no obvious change in substrate acoustic impedance along the channel, which suggests that lithological contrasts do not play an important role in determining the shape of Bressay river

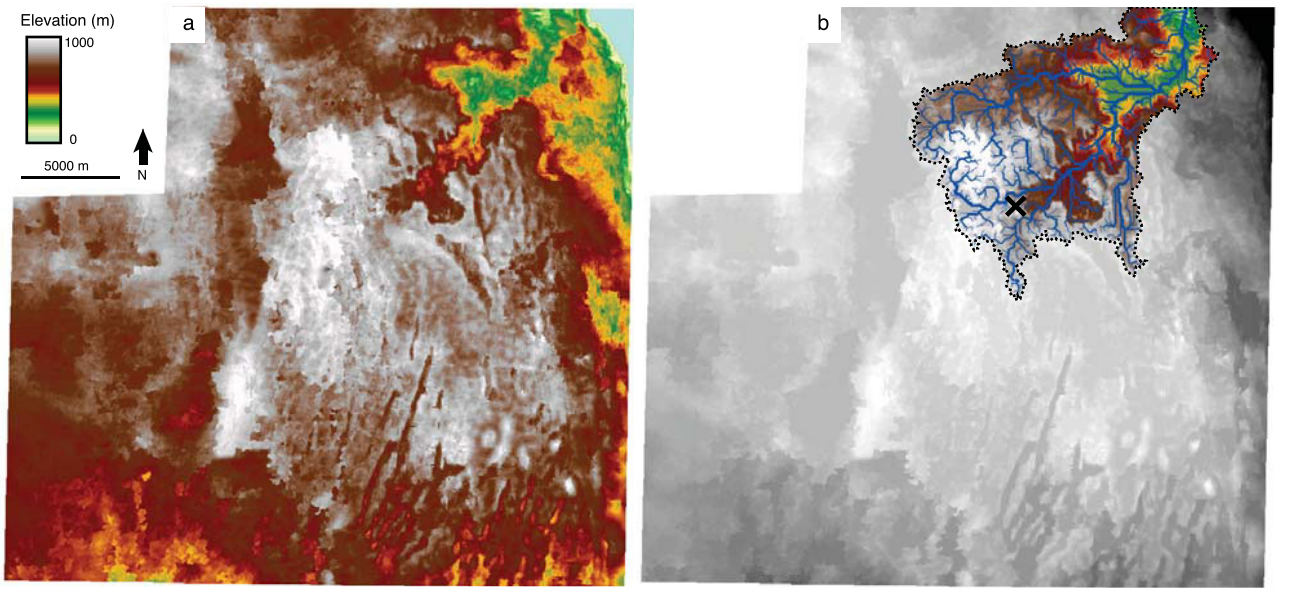

Figure 10. (a) Depth converted and decompacted Bressay landscape. (b) Drainage divide (black) and mapped rivers (blue) extracted from Bressay landscape. Outside of Bressay drainage basin is shown as gray scale. Black cross = location of river shown in Figures 11b and 11c.

profiles. Instead, we suggest that this landscape was generated by base-level change (uplift) and erosion 58–55 million years ago.

The gamma-ray log of well 3/28a-4 intersects the channel infill and is shown as an inset in Figure 11c. The well log and seismic data are consistent with burial first by sand (e.g., Figure 5a; core interval: 1050–1070 m, gamma-ray values: 20–30 gAPI) and then by alternating marine shales (core interval: 1100–1120 m, gamma-ray values >100 gAPI) and sand. We suggest that these observations are consistent with burial first by terrestrial clastic material and that subsequent drowning was staged. The age of dinocysts contained in the underlying and overlying deltaic deposits (Dornoch and Stronsay Formations) constrain the duration of formation of the Bressay landscape to <3 Ma. Relief from drainage patterns extracted from this landscape indicates that the Bressay region was uplifted by at least 350 m. The shapes of the river profiles extracted from the Bressay landscape imply that uplift was episodic and that inverting for an uplift rate history might be fruitful.

2.8. Inverting for Uplift Rate

Pritchard et al. [2009] and *Roberts and White* [2010] first showed that longitudinal river profiles could be successfully inverted for a history of uplift rate. We use a simplified version of the stream power model to invert rivers draining the Bressay landscape for uplift, U, as a function of time, t,

$$\frac{\partial z}{\partial t} = U(t) - vA(x)^m \frac{\partial z}{\partial x}, \tag{5}$$

where erosion rate is parameterized using the advective term on the right-hand side of equation (5) [*Rosenbloom and Anderson*, 1994; *Whipple and Tucker*, 1999]. This term controls the velocity of kinematic erosional waves as they propagate upstream. Velocities depend on upstream drainage area, A, which is measured from the extracted landscape and the values of the erosional parameters, v and m, which are constrained by the landscape exposure duration. The biostratigraphic records discussed in section 2.3 indicate that the duration of exposure is <3 Ma. We use a central value of 1.5 Ma. A joint inversion of the drainage inventory indicates that best fitting $m = 0.5$, and a landscape response time of 1.5 Ma yields $v = 1.6$ Ma^{-1} [e.g., *Rudge et al.*, 2015]. The inverse problem can be solved by seeking the minimum value of an objective function, H, that incorporates data (rms) misfit, model roughness, and a positivity penalty function, P,

$$H = \left[\frac{1}{N}\sum_{i=1}^{N}\left(\frac{z_i^o - z_i^c}{\sigma_i}\right)^2\right]^{\frac{1}{2}} + w\left(\frac{\mathrm{d}U}{\mathrm{d}t} + \frac{\mathrm{d}^2U}{\mathrm{d}t^2}\right) + P, \tag{6}$$

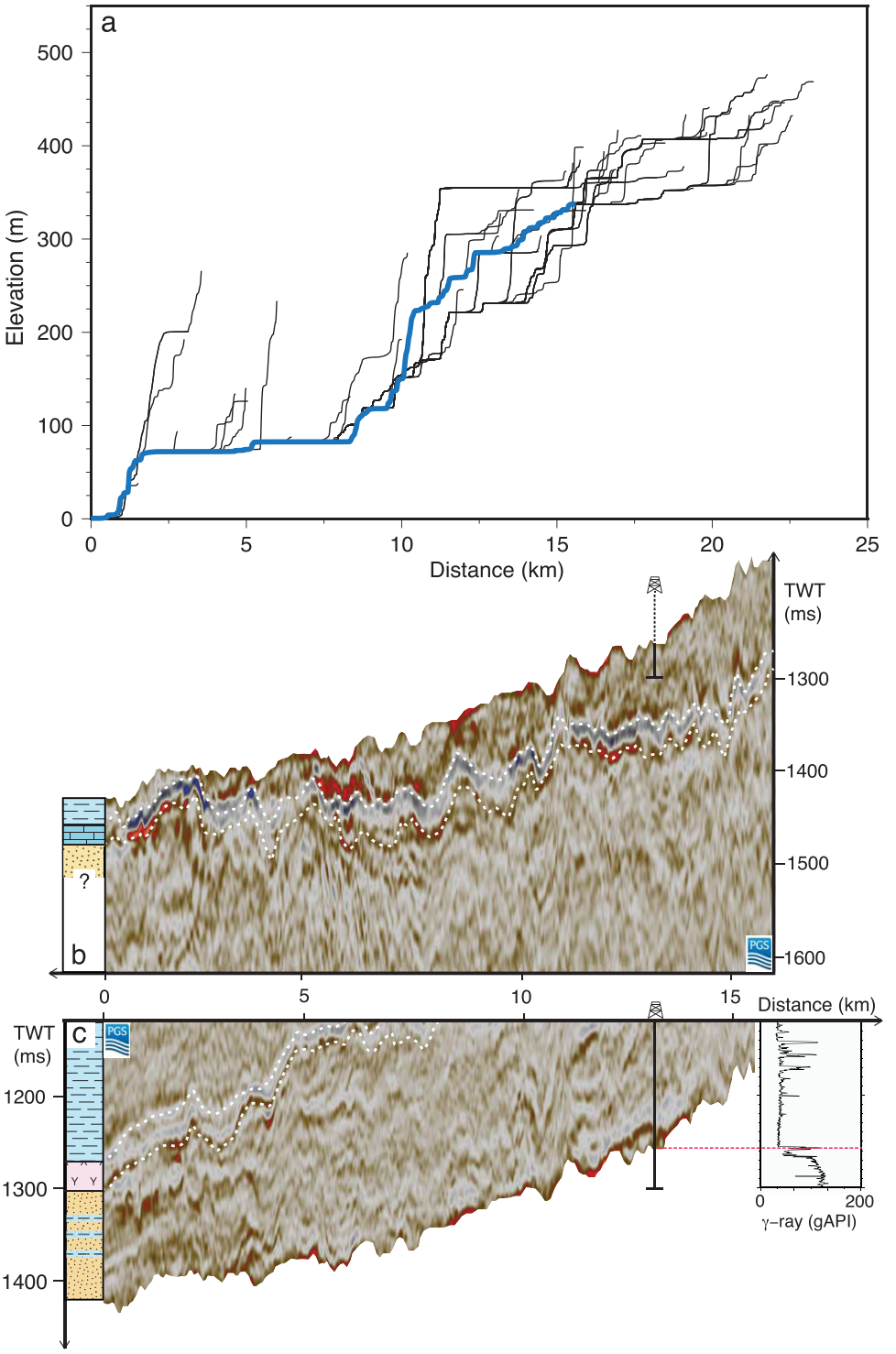

Figure 11. (a) Longitudinal profiles of 87 rivers in the Bressay region. (b) Seismic and stratigraphic data extracted beneath the river shown in blue in Figure 11a (see cross in Figure 10b). TWT = two-way time. (c) Seismic and stratigraphic data extracted above the blue colored river in Figure 11a. White dotted lines = stratigraphic boundaries. Gamma-ray values for the deepest portion of well 3/28a-4 intersecting the river are shown to the right. gAPI > 100 indicate mudstones and gAPI < 100 suggest sandier lithologies.

where N is the total number of measurements of elevation and distance in our drainage inventory [*Roberts and White*, 2010]. We set data variance σ_i to 20 m, which is a conservative estimate of the vertical resolution of the seismic data. In practice, we seek the smoothest uplift rate history that yields the lowest residual

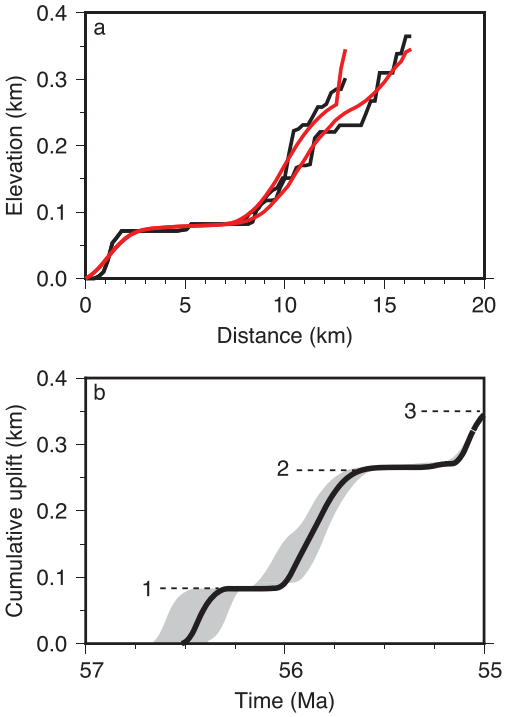

Figure 12. Joint inversion of two main tributaries for uplift rate as a function of time. (a) Black = observed river profiles. Red = best fitting theoretical profiles. (b) Cumulative uplift history that produced theoretical profiles in Figure 12a. Gray band = range of uplift histories for erosional parameter $v = 1.6 \pm 0.1$ Ma^{-1}. Uplift events are labeled 1, 2, 3.

misfit between observed and theoretical river profiles [*Parker*, 1994]. In this study, smoothing parameter $w = 0.1$. We use Powell's algorithm, a conjugate gradient method, to invert for uplift rate histories, which yields stable solutions [*Roberts and White*, 2010; *Hartley et al*., 2011].

3. Vertical Motions of Bressay Between 58 and 55 Ma

Well reports, presence of angiosperm debris in core samples, dinocyst biostratigraphy, and remapping of stratigraphy using PGS's three-dimensional BBK survey indicate that the Bressay region was uplifted, eroded by a fluvial drainage network, and then rapidly drowned between 58 and 55 Ma. The erosional landscape was extracted by mapping a stratigraphic unconformity, which is overlain by the conglomeratic Bressay Sandstone, the sandy Dornoch Formation, the Balder Formation, and the marine Stronsay Group. These observations show that total cumulative (i.e., peak) uplift occurred before 54.8 Ma (i.e., youngest reported age of *A.a*), suggesting it is older than previously thought [cf. *Underhill*, 2001; *Rudge et al*., 2008]. We used check-shot data to convert seismic data to depth and to parameterize decompaction. Importantly, our estimate of maximum relief is 100–150 m more than in *Underhill* [2001], which we attribute to better seismic data, mapping of every inline and cross line, and a reevaluation of biostratigraphic data.

We inverted the shapes of longitudinal river profiles draining the Bressay landscape for a history of uplift rate. The calculated uplift history from a joint-inversion of the two main rivers is shown in Figure 12. Residual rms misfit is 0.64. Calculated uplift rate history has three phases of increased uplift, labeled 1, 2, 3 in Figure 12b. The magnitudes of the uplift events are 100–200 m and total cumulative uplift exceeds 350 m. Calculated uplift rates are 0.5–1 mm/a, with uplift beginning at 56.5 Ma and culminating at 55.0 Ma. Gray band in Figure 12b shows uncertainty in calculated uplift for $v = 1.6 \pm 0.1$ Ma^{-1}. If $v = 4.75$ Ma^{-1} [cf. *Hartley et al*., 2011] calculated uplift occurs within <1 Ma of peak uplift. A three-stage uplift history was also observed in the Judd region of the Faeroe-Shetland basin (see Figure 13a). In Judd, cumulative uplift reached $\sim$900 m and the landscape was exposed subaerially for $\sim$2.5 Ma, with peak uplift between 56.1 and 55.0 Ma [*Shaw-Champion et al*., 2008; *Rudge et al*., 2008; *Hartley et al*., 2011]. Rapid postuplift subsidence drowned the Bressay and Judd regions.

An important source of uncertainty is the velocity model, used to convert two-way time to depth, and the compaction parameterisation. We covaried velocity models and compaction parameters within the uncertainties shown in Figures 9a and 9c to test their impact on calculated uplift histories (i.e., fastest, best fitting, slowest velocity models and most compacted, best fitting, least compacted models). We then reran the flow routing algorithms for each of these nine landscapes and reextracted their drainage patterns. The planforms of the nine drainage networks are very similar. River elevations are stretched or compressed vertically by ± 25 m depending on the velocity and compaction parameters chosen. The location and relief of knickzones are largely unaffected by these uncertainties. These tests indicate that the extracted drainage network and calculated uplift rate history are insensitive to geophysical uncertainties.

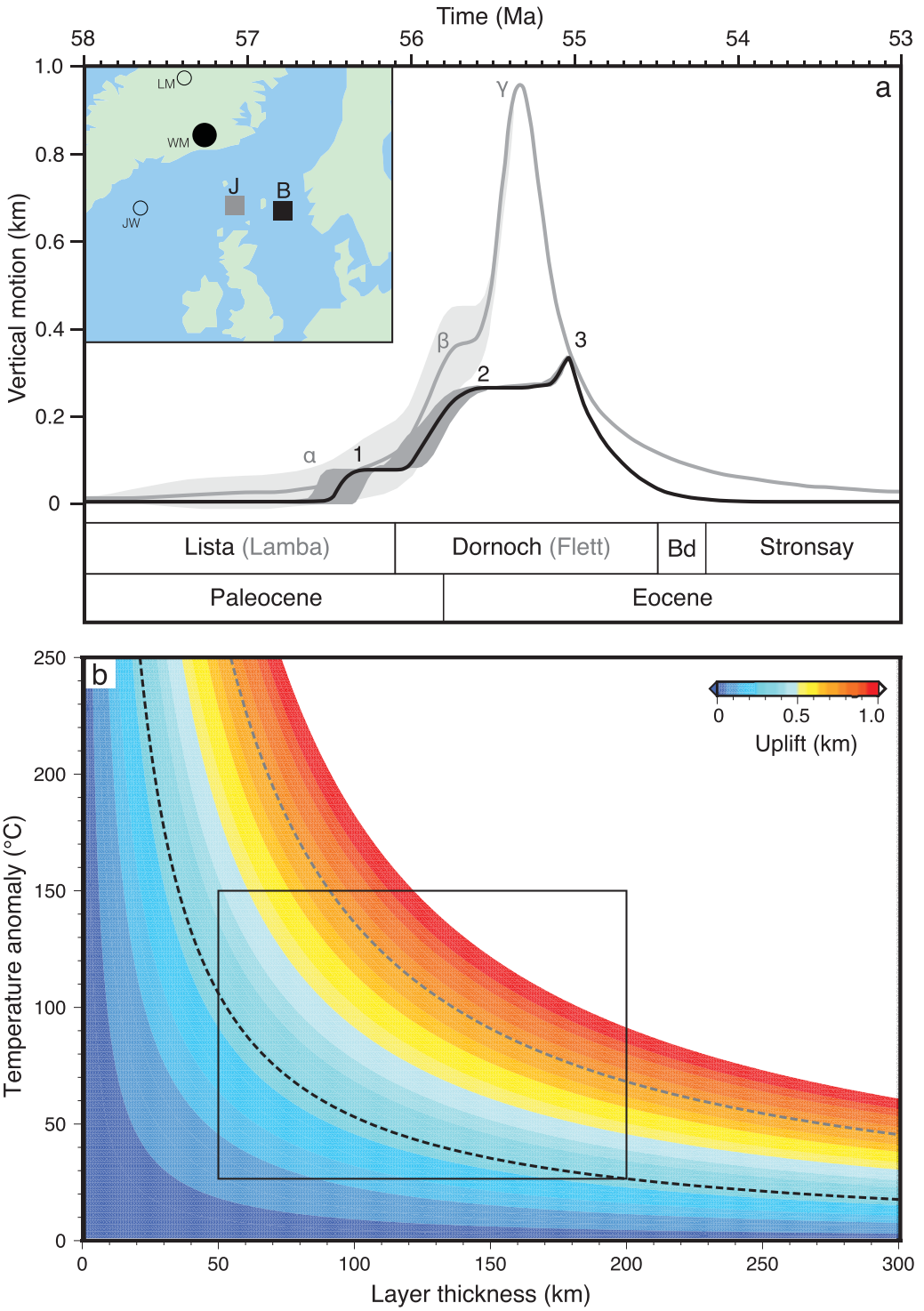

Figure 13. (a) Uplift histories for Bressay (black) and Judd (gray) [*Hartley et al.*, 2011]. Gray bands = uncertainty from erosional parameter values. 1, 2, and 3 = Bressay uplift events. α, β, γ = Judd uplift events. Inset = Paleocene-Eocene paleogeography showing location of uplifted regions: black square = Bressay; gray square = Judd; red circle (WM) = Icelandic plume center from *White and McKenzie* [1989]; LM/JW = plume centers from *Lawver and Muller* [1994] and *Jones and White* [2003]. (b) Uplift as a function of excess temperature and thickness of low viscosity channel beneath the plate. Black dashed line = 350 m of uplift (Bressay), gray dashed line = 900 m of uplift (Judd). Note strong trade-off between layer thickness and thermal anomaly. Black square denotes geologically reasonable ranges for layer thickness and excess temperature from *Rudge et al.* [2008].

4. Discussion

We consider four processes that could have generated the rapid Paleocene-Eocene vertical motions observed: glacio-eustasy, underplating, crustal shortening, and mantle convection.

Glacio-eustasy can generate rapid base level changes when polar ice is present. However, there was probably little polar ice during the Paleocene-Eocene Thermal Maximum (PETM) when glacio-eustatic sea level probably varied by a few tens of meters at most (Figure 2) [*Haq et al*., 1988; *Miller et al*., 2005]. The growth of relief in the Bressay region appears to be local to the East Shetland Platform, which also indicates that glacio-eustasy is not responsible generating the base level changes observed.

If we assume that isostasy applies, a simple isostatic calculation shows that underplating generates air-loaded uplift, $e=t_u(\rho_a-\rho_u)/\rho_a$, where ρ_a and ρ_u are respective densities of mantle (3.2 g/cm^3) and underplate, and t_u is underplate thickness. Using $2.72 \leq \rho_u \leq 2.9$ g/cm^3, which represent the range of densities expected for molten to solid (gabbroic) underplate, yields $0.09t_u \leq e \leq 0.15t_u$ [*Maclennan and Lovell*, 2002]. These simple equations indicate that net uplift following solidification of underplated material is expected to be ~60% of initial uplift, which does not match the rapid postuplift net subsidence we observe. Moreover, to generate the 350 m of uplift we observe >2 km of underplate is required. If a large amount of underplating occurred, we expect to see evidence of melting (e.g., dykes, sills) in well and seismic data. The well and seismic data contain no evidence of magmatism or significant shortening (e.g., Figures 6 and 7). The proximity of Judd and Bressay to the Icelandic plume at ~55 Ma indicate that subplate support might have played the key role in generating uplift and subsidence.

Stretched and subsided continental lithosphere, such as the Paleocene northern North Sea, has an elastic thickness of a few kilometers, which means that short wavelength changes in subplate support should generate observable vertical motions at Earth's surface [*Ziegler*, 1992; *Tiley et al*., 2003; *Rudge et al*., 2008]. To investigate the mantle flow required to generate observed uplift and subsidence, we calculate excess temperature anomalies and explore the implications for mantle flow using the reinterpreted age of the Bressay landscape. Surface uplift, U, from a subplate thermal anomaly, $\bar{T}$, can be estimated using a simple isostatic calculation,

$$U=\frac{2h\alpha\bar{T}}{1-\alpha T_\circ}, \tag{7}$$

where $2h$ is thickness of the anomalously hot layer, $T_\circ$ is background temperature, and thermal expansion coefficient $\alpha=3.3\times10^{-5}\,^\circ\mathrm{C}^{-1}$ [*Rudge et al*., 2008]. If, for example, the background temperature of the plume was 1400°C (~100–200°C greater than normal) and the thickness of the anomalously hot layer is 200 km, the excess temperature, $\bar{T}$, required to produce 350 m of uplift (i.e., peak Bressay uplift) is 50°C. Inspection of equation (7) shows that uplift is insensitive to background temperature. Using a background temperature of 1200°C, for example, changes calculated excess temperature by <1°C. Results are much more sensitive to the thickness of the hot layer. For example, a 100 km thick layer yields excess temperatures of 100°C. The upper bound for the temperature of the pulse beneath Bressay is therefore 1450–1500°C, which is unlikely to have generated much melt beneath modestly stretched lithosphere [*White and McKenzie*, 1989]. Figure 13b shows the trade-off between the layer thickness and the thermal anomaly. Peak uplift from the Judd area is ~900 m, which indicates a thermal anomaly of 130°C for a 200 km thick channel [*Hartley et al*., 2011]. Higher temperatures beneath Judd relative to Bressay are consistent with its closer proximity to the plume center (see inset in Figure 13a). Following uplift these regions subsided rapidly in 0.5–1 Ma.

Drainage patterns of Bressay and Judd contain three knickzones that are consistent with a three-stage uplift history (e.g., Figure 13a). The similarity of both uplift histories suggests that they share a common mechanism. *Hartley et al*. [2011] suggested that the three-stage uplift history of Judd was generated by the passage of thermo-chemical pulses beneath the plate originating from the Icelandic plume. The passage of thermal anomalies in a hot channel beneath the plate is attractive because it provides a mechanism for rapid uplift and subsidence. Detailed fluid dynamical modeling [e.g., *Larsen et al*., 1999] is beyond the scope of this paper; instead, we modify *Rudge et al*. [2008]'s one-dimensional radial advection model and use our estimates of the time of peak uplift to calculate the age at which the putative thermal anomaly departed the plume center. Uplift in both regions must have occurred after 58.0 Ma (age of *A.m*. in underlying stratigraphy). Supposing that uplift in Judd and Bressay was generated by the passage of a thermal anomaly it must have travelled between Judd and Bressay before 54.8–55.8 Ma (i.e., age of *A.a* in the Bressay Dornoch

Formation). Our observations indicate that the timing of peak uplift in Bressay and Judd is closer than previously thought [cf. *Rudge et al*., 2008]. The difference in age between Bressay and Judd peak uplift is determined by the age of *A.a* (55.8–54.8 Ma) and the age of infill of Judd stratigraphy constrained by dating of pollen spores (56.1–55.0 Ma) [*Shaw-Champion et al*., 2008].

Conservation of mass means that velocity, $u \propto 1/r$, and position of a pulse, r, at a time, t, can be expressed as,

$$r^2(t) = k(t - t_\circ), \tag{8}$$

where $t_\circ$ is the time the pulse leaves its origin [*Rudge et al*., 2008]. k characterizes the speed of the pulse and has units of diffusivity. Since we have information about uplift at two different positions, we can estimate k using,

$$k = \frac{r_B^2 - r_J^2}{t_B - t_J}, \tag{9}$$

where r_B and t_B represent the position and age of peak Bressay uplift, respectively. r_J and t_J are the corresponding parameters for Judd. As $k \propto r^2$, calculated departure time depends strongly on the location of the plume head. Using *White and McKenzie* [1989]'s plume center, $r_J = 580$ km and $r_B = 820$ km. However using *Lawver and Muller* [1994]'s plume center, $r_J = 1070$ km and $r_B = 1260$ km, and using *Jones and White* [2003]'s plume center we obtain $r_J = 770$ km and $r_B = 1100$ km (see inset in Figure 13a).

Using the uncertainty in age of peak uplift in Judd and the youngest possible age of the Bressay landscape yields $0.2 \leq t_B - t_J \leq 1.3$ Ma. We then use the uncertainty in the location of the plume center to obtain three different values for $r_B^2 - r_J^2$ for each of the plume centers. Using equation (9) we obtain three different values for k for each plume center. Rearranging equation (8) and inserting the range of k and radii values from the respective plume centers indicates that the latest time a thermal pulse could have left the plume center to generate the Bressay and Judd landscapes is $t_\circ = 57.4 \pm 2.2$ Ma. We suggest that the passage of thermo-chemical pulses from the Icelandic plume could have generated the Paleocene—Eocene vertical motions observed in Bressay and Judd. Our reinterpreted age of the Bressay landscape indicates that these thermal anomalies travelled between Bressay and Judd at rates in excess of ~150 km/Ma, which is similar to the mantle flow velocities calculated using the geometry of the V-shaped ridges south of Iceland [*Jones et al*., 2002b]. The simple model used indicates that thermal anomalies directly beneath the plate can travel orders of magnitude faster than plate velocities.

5. Conclusion

We interpreted data from seven wells, a three-dimensional seismic survey, and inverted drainage patterns to reconstruct the uplift history of an ancient Paleogene landscape buried beneath the Bressay region of the northern North Sea. The first and last occurrences of the marine dinocysts *Apectodinium augustum* and *Alisocysta margarita* in underlying and overlying stratigraphy indicate that this landscape formed between 58 and 55 Ma. Geochemical analyses of cuttings from an interval that includes the erosional surface contain angiosperm (flower plant) debris. Core samples and gamma-ray logs from wells that intersect mapped channels indicate that the landscape was first buried by terrestrial-derived clastic material and then by marine mudstones.

These observations combined with fluvial drainage patterns, beach ridges, and a paleo-coastline mapped using the three-dimensional seismic volume indicate that the erosional surface was generated subaerially and then rapidly submerged. Check-shot data were used to depth-convert and decompact the buried landscape and flow routing algorithms were used to extract drainage patterns from the landscape. The extracted longitudinal river profiles have three knickzones and a relief of ~350 m. Hundreds of meters of relief, a lack of evidence for shortening in seismic data, and rapid subsidence indicate that lithospheric shortening, glacio-eustasy, and underplating did not create this erosional landscape. River profile shapes are similar to those extracted from a slightly older buried landscape in the Judd region ~400 km to the west. We inverted the longitudinal profiles of the two main rivers for an uplift rate history.

The best fitting history has three phases of high uplift rates (>0.5 mm/a), which are slightly smaller than those calculated using the Judd rivers. We suggest that these observations are consistent with passage of thermo-chemical pulses during inception of the Icelandic plume. The reconstructed uplift history of Bressay contains

important information about the velocity and temperature of thermochemical convection generated by the plume. Simple isostatic calculations indicate that the maximum thermal anomalies beneath Judd and Bressay were ~130 and 50°C, respectively. A simple model of radial subplate flow suggests that these thermal anomalies departed the plume center as late as 57.4 ± 2.2 Ma and traveled with a velocity in excess of ~150 km/Ma.

Mapping of ancient buried landscapes is a rich source of geomorphological and geodynamic information and can be used to constrain the temporal and spatial evolution of mantle convective processes.

Appendix A: Biostratigraphic Markers of the Paleocene-Eocene Boundary

Biostratigraphic markers used for construction of Bressay chronostratigraphic chart in Figure 2 are listed in Table A1. Note that A.a. and A.m., key dinocysts used to constrain Bressay unconformity, have different age ranges depending on literature.

Table A1. Dinoflagellate Cyst Biomarkers of the Paleocene-Eocene Boundary in the Bressay Region

Abbreviation	Nomenclature	Depth(m)	Age
A.d.	*Areosphaeridium diktyoplokum*	930–1110	E.-L. Eocene [*Williams and Bujak*, 1989]
T. d	*Thalassiphora delicata*	1000–1140	L. Paleocene-M. Eocene [*Williams and Bujak*, 1989]
D.o.	*Deflandrea oebisfeldensis*	1060–1130	L. Paleocene-E. Eocene [*Williams and Bujak*, 1989]
H.t.	*Hystrichosphaeridium tubiferum*	980–1100	E.-M. Eocene [*Williams and Bujak*, 1989]
D.p	*Deflandrea phosphoritica*	1000–1180	Eocene-Oligocene [*Williams and Bujak*, 1989]
W.a	*Wetzelliela articulata*	1000–1200	Eocene [*Williams and Bujak*, 1989]
L.w.	*Lentinia wetzelii*	1020–1110	E. Eocene [*Williams and Bujak*, 1989]
H.p.	*Homotryblium pallidum*	1040–1130	Eocene-E. Oligocene [*Williams and Bujak*, 1989]
A.h.	*Apectodinium homorphum*	1070–1190	L. Paleocene-M. Eocene [*Williams and Bujak*, 1989]
A.a.	*Apectodinium augustum*	1180–1190	54.8–55.3 Ma [*Mudge and Bujak*, 2001] 54.8–55.8 Ma [*Luterbacher et al.*, 2004] 55.8–56.5 Ma [*Vandenberghe et al.*, 2012]
G.o.	*Glaphyrocysta ordinata*	1120–1360	L. Paleocene-E. Eocene [*Williams and Bujak*, 1989]
P.p.	*Palaeoperidinium pyrophorum*	1290–1460	Maastrichtian-L. Paleocene [*Williams and Bujak*, 1989]
C.s.	*Ceratiopsis speciosa*	1290–1460	Maastrichtian-L. Paleocene [*Williams and Bujak*, 1989]
A.m.	*Alisocysta margarita*	1000–1470	56.2–? Ma [*Mudge and Bujak*, 2001] 58.0–59.2 Ma [*Luterbacher et al.*, 2004] ?–59.7 Ma [*Vandenberghe et al.*, 2012]

Acknowledgments
This work was supported by a studentship from the National Environmental Research Council (NERC) and a grant from the London Petrophysical Society. We thank P.G.S. for permission to display seismic reflection profiles from the BBK data set. All seismic reflection and well data were made available through PGS and Statoil. We are grateful for core samples and photographic data which were obtained freely through the British Geological Survey at Keyworth. We thank R. Bell, P. Burgess, G. Hampson, L. Lonergan, M. Sephton, T. Weight, and N. White for helpful discussion. T. Becker, J. Chalmers, and an anonymous reviewer are thanked for their constructive comments. Data, input files, and source code necessary to reproduce uplift inversion model results are available from the authors upon request (g.stucky-de-quay14@imperial.ac.uk; gareth.roberts@imperial.ac.uk).

References

Adedosu, T. A., O. O. Sonibare, O. Ekundayo, and J. Tuo (2010), Hydrocarbon-generative potential of coal and interbedded shale of Mamu Formation, Benue Trough, Nigeria, *Pet. Sci. Technol.*, *28*(4), 412–427, doi:10.1080/10916460902725306.

Allen, R. M., et al. (2002), Imaging the mantle beneath Iceland using integrated seismological techniques, *J. Geophys. Res.*, *107*(B12), 1–16, doi:10.1029/2001JB000595.

Andrews, I., D. Long, P. Richards, A. Thomson, S. Brown, J. Chesher, and M. McCormac (1990), United Kingdom offshore regional report: The geology of the Moray Firth, *96*, Br. Geol. Surv., HMSO, London, U. K.

Anell, I., H. Thybo, and I. M. Artemieva (2009), Cenozoic uplift and subsidence in the North Atlantic region: Geological evidence revisited, *Tectonophysics*, *474*, 78–105, doi:10.1016/j.tecto.2009.04.006.

Breddam, K., M. D. Kurz, and M. Storey (2000), Mapping out the conduit of the Iceland mantle plume with helium isotopes, *Earth Planet. Sci. Lett.*, *176*, 45–55, doi:10.1016/S0012-821X(99)00313-1.

Christensen, N. I. (1982), Seismic velocities, in *Handbook of Physical Properties of Rocks*, vol.II, edited by R. S. Carmichael, pp. 57–74, CRC Press, Boca Raton, Fla.

Cramer, B. S., J. R. Toggweiler, J. D. Wright, M. E. Katz, and K. G. Miller (2009), Ocean overturning since the Late Cretaceous: Inferences from a new benthic foraminiferal isotope compilation, *Paleoceanography*, *24*, 1–14, doi:10.1029/2008PA001683.

Czarnota, K., M. J. Hoggard, N. White, and J. Winterbourne (2013), Spatial and temporal patterns of Cenozoic dynamic topography around Australia, *Geochem. Geophys. Geosyst.*, *14*, 634–658, doi:10.1029/2012GC004392.

Darbyshire, F. A., K. F. Priestley, R. S. White, R. Stefánsson, G. B. Gudmundsson, and S. S. Jakobsdóttir (2000), Crustal structure of central Iceland from analysis of teleseismic receiver functions, *Geophys. J. Int.*, *143*, 163–184, doi:10.1046/j.1365-246x.2000.00224.x.

Dam, G., M. Larsen, and M. Sonderholm (1998), Sedimentary response to mantle plumes: Implications from Paleocene onshore successions, West and East Greenland, *Geology*, *26*(3), 207–210.

Dziewonski, A. M., and D. L. Anderson (1981), Preliminary reference Earth model, *Phys. Earth Planet. Inter.*, *25*(4), 297–356.

Einarsson, P. (1991), Earthquakes and present day tectonism in Iceland, *Tectonophysics*, *189*, 261–279, doi:10.1016/0040-1951(91)90501-I.

Eneogwe, C., O. Ekundayo, and B. Patterson (2002), Source-derived oleanenes identified in Niger Delta oils, *J. Pet. Geol.*, *25*(1), 83–95, doi:10.1111/j.1747-5457.2002.tb00100.x.

Förste, C., S. Bruinsma, O. Abrikosov, J.-M. Lemoine, J. C. Marty, F. Flechtner, G. Balmino, F. Barthelmes, and R. Biancale (2014), EIGEN-6C4 The Latest Combined Global Gravity Field Model Including GOCE Data Up to Degree and Order 2190 of GFZ Potsdam and GRGS Toulouse, GFZ Data Serv., Potsdam, Germany, doi:10.5880/icgem.2015.1.

Gradstein, F. M., I. L. Kristiansen, L. Loemo, and M. A. Kaminski (1992), Cenozoic foraminiferal and dinoflagellate cyst biostratigraphy of the central North Sea, *Micropaleontology*, *38*(2), 101–137, doi:10.2307/1485991.
Green, P. F., Lidmar-Bergstrom, K., Japsen, P., Bonow, J. M., Chalmers, J. A. (2013), Stratigraphic landscape analysis, thermochronology and the episodic development of elevated, passive continental margins, *Geol. Surv. Den. Greenl. Bull.*, *30*, 150 pp.
Haq, B. U., J. Hardenbol, and P. R. Vail (1988), Mesozoic and Cenozoic chronostratigraphy and eustatic cycles, in *Sea-Level Changes—An Integrated Approach*, vol. 42, pp. 71–108, SEPM Special Publications, Tulsa, Oklahoma, doi:10.2110/pec.88.01.0071.
Hartley, R., G. G. Roberts, N. White, and C. Richardson (2011), Transient convective uplift of an ancient buried landscape, *Nat. Geosci.*, *4*, 562–565, doi:10.1038/ngeo1191.
Hoggard, M. J., N. White, and D. Al-Attar (2016), Global dynamic topography observations reveal limited influence of large-scale mantle flow, *Nat. Geosci.*, *9*, 456–465, doi:10.1038/ngeo2709.
Jackson, C. A.-L., H. Grunhagen, J. A. Howell, A. L. Larsen, A. Andersson, F. Boen, and A. Groth (2010), 3D seismic imaging of lower delta-plain beach ridges: Lower Brent Group, northern North Sea, *J. Geol. Soc.*, *167*(6), 1225–1236, doi:10.1144/0016-76492010-053.
Japsen, P., and J. A. Chalmers (2000), Neogene uplift and tectonics around the North Atlantic: Overview, *Global Planet. Change*, *24*, 165–173, doi:10.1016/S0921-8181(00)00006-0.
Jones, R. W., and N. J. Milton (1994), Sequence development during uplift: Palaeogene stratigraphy and relative sea-level history of the Outer Moray Firth, UK North Sea, *Mar. Pet. Geol.*, *11*(2), 157–165, doi:10.1016/0264-8172(94)90092-2.
Jones, S. M., N. White, B. J. Clarke, E. Rowley, and K. Gallagher (2002a), Present and past influence of the Iceland Plume on sedimentation, *Geol. Soc. Spec. Publ.*, *196*, 13–25, doi:10.1144/GSL.SP.2002.196.01.02.
Jones, S. M., N. White, and J. Maclennan (2002b), V-shaped ridges around Iceland: Implications for spatial and temporal patterns of mantle convection, *Geochem. Geophys. Geosyst.*, *3*(10), 1059, doi:10.1029/2002GC000361.
Jones, S. M., and N. White (2003), Shape and size of the starting Iceland plume swell, *Earth Planet. Sci. Lett.*, *216*, 271–282, doi:10.1016/S0012-821X(03)00507-7.
Knox, R. W. O., and A. C. Morton (1988), The record of early Tertiary N Atlantic volcanism in sediments of the North Sea Basin, *Geol. Soc. Spec. Publ.*, *39*(1), 407–419, doi:10.1144/GSL.SP.1988.039.01.36.
Knox, R. W. O., and S. Holloway (1992), Paleogene of the central and Northern North Sea, in *Lithostratigrphic Nomenclature of the UK North Sea*, edited by R. W. O. Knox and W. G. Cordey, pp. 1–160, Br. Geol. Surv., Nottingham, U. K.
Larsen, T. B., D. A. Yuen, and M. Storey (1999), Ultrafast mantle plumes and implications for flood basalt volcanism in the Northern Atlantic Region, *Tectonophysics*, *311*, 31–43, doi:10.1016/S0040-1951(99)00163-8.
Lawver, L. A., and R. D. Muller (1994), Iceland hotspot track, *Geology*, *22*, 311–314, doi:10.1130/0091-7613(1994)022<0311:IHT>2.3.CO;2.
Liu, X., and W. E. Galloway (1997), Quantitative determination of tertiary sediment supply to the North Sea Basin, *AAPG Bull.*, *81*(9), 1482–1509.
Luterbacher, H. P., J. R. Ali, H. Brinkhuis, F. M. Gradstein, J. J. Hooker, S. Monechi, J. G. Ogg, J. Powell, U. Rohl, A. Sanfilippo, and B. Schmitz (2004), The Paleogene period, in *A Geologic Time Scale 2004*, edited by F. M. Gradstein, J. G. Ogg, and A. G. Smith, pp. 384–408, Cambridge Univ. Press, Cambridge, U. K., doi:10.1017/CBO9780511536045.021.
Mackay, L. M., J. Turner, S. M. Jones, and N. J. White (2005), Cenozoic vertical motions in the Moray Firth Basin associated with initiation of the Iceland Plume, *Tectonics*, *24*, 1–23, doi:10.1029/2004TC001683.
Maclennan, J., and B. Lovell (2002), Control of regional sea level by surface uplift and subsidence caused by magmatic underplating of Earth's crust, *Geology*, *30*(8), 675–678, doi:10.1130/0091-7613(2002)030<0675:CORSLB>2.0.CO;2.
Matthews, S., O. Shorttle, and J. Maclennan (2016), The temperature of the Icelandic mantle from olivine-spinel aluminum exchange thermometry, *Geochem. Geophys. Geosyst.*, *17*, 4725–4752, doi:10.1002/2016GC006497.
McKenzie, D. (2010), The influence of dynamically supported topography on estimates of Te, *Earth Planet. Sci. Lett.*, *295*, 127–138.
Medvedev, S., A. Souche, and E. H. Hartz (2013), Influence of ice sheet and glacial erosion on passive margins of Greenland, *Geomorphology*, *193*, 36–46.
Miller, K. G., M. A. Kominz, J. V. Browning, J. D. Wright, G. S. Mountain, M. E. Katz, P. J. Sugarman, B. S. Cramer, N. Christie-Blick, and S. F. Pekar (2005), The Phanerozoic record of global sea-level change, *Science*, *310*(5752), 1293–1298, doi:10.1126/science.1116412.
Mudge, D. C. (2015), Regional controls on Lower Tertiary sandstone distribution in the North Sea and NE Atlantic margin basins, *Geol. Soc. Spec. Publ.*, *403*, 17–42, doi:10.1144/SP403.5.
Mudge, D., and J. Bujak (1994), Eocene stratigraphy of the North Sea Basin, *Mar. Pet. Geol.*, *11*(2), 166–181, doi:10.1016/0264-8172(94)90093-0.
Mudge, D., and J. Bujak (1996), An integrated stratigraphy for the Paleocene and Eocene of the North Sea, *Geol. Soc. Spec. Publ.*, *101*, 91–113.
Mudge, D. C., and J. P. Bujak (2001), Biostratigraphic evidence for evolving palaeoenvironments in the Lower Paleogene of the Faeroe-Shetland Basin, *Mar. Pet. Geol.*, *18*(5), 577–590, doi:10.1016/S0264-8172(00)00074-X.
Mudge, D. C., and P. Copestake (1992), Lower Palaeogene stratigraphy of the northern North Sea, *Mar. Pet. Geol.*, *9*(3), 287–301, doi:10.1016/0264-8172(92)90077-R.
Mudge, D. C., and S. M. Jones (2004), Palaeocene uplift and subsidence events in the Scotland-Shetland and North Sea region and their relationship to the Iceland Plume, *J. Geol. Soc.*, *161*(3), 381–386, doi:10.1144/0016-764903-038.
Neal, J. E. (1996), A summary of Paleogene sequence stratigraphy in northwest Europe and the North Sea, *Geol. Soc. Spec. Publ.*, *101*(1), 15–42, doi:10.1144/GSL.SP.1996.101.01.02.
Óskarsson, N., S. Steinthórsson, and G. E. Sigvaldason (1985), Iceland geochemical anomaly: Origin, volcanotectonics, chemical fractionation and isotope evolution of the crust, *J. Geophys. Res.*, *90*(B12), 10,011–10,025, doi:10.1029/JB090iB12p10011.
Parker, R. L. (1994), *Geophysical Inverse Theory*, Princeton Univ. Press, Princeton, N. J.
Parkin, C. J., Z. C. Lunnon, R. S. White, P. A. F. Christie, and iSIMM team (2007), Imaging the pulsing Iceland mantle plume through the Eocene, *Geology*, *35*(1), 93–96, doi:10.1130/G23273A.1.
Parnell-Turner, R., N. White, T. Henstock, B. Murton, J. Maclennan, and S. M. Jones (2014), A continuous 55-million-year record of transient mantle plume activity beneath Iceland, *Nat. Geosci.*, *7*(12), 914–919, doi:10.1038/ngeo2281.
Poore, H. R., N. White, and S. Jones (2009), A Neogene chronology of Iceland plume activity from V-shaped ridges, *Earth Planet. Sci. Lett.*, *283*, 1–13, doi:10.1016/j.epsl.2009.02.028.
Poore, H., N. White, and J. Maclennan (2011), Ocean circulation and mantle melting controlled by radial flow of hot pulses in the Iceland plume, *Nat. Geosci.*, *4*(8), 558–561, doi:10.1038/ngeo1161.
Pritchard, D., G. G. Roberts, N. J. White, and C. N. Richardson (2009), Uplift histories from river profiles, *Geophys. Res. Lett.*, *36*, doi:10.1029/2009GL040928.

Rickers, F., A. Fichtner, and J. Trampert (2013), The Iceland-Jan Mayen plume system and its impact on mantle dynamics in the North Atlantic region: Evidence from full-waveform inversion, *Earth Planet. Sci. Lett.*, *367*, 39–51, doi:10.1016/j.epsl.2013.02.022.
Roberts, G. G., and N. White (2010), Estimating uplift rate histories from river profiles using African examples, *J. Geophys. Res.*, *115*, doi:10.1029/2009JB006692.
Röhl, U., T. Westerhold, T. J. Bralower, and J. C. Zachos (2007), On the duration of the Paleocene-Eocene thermal maximum (PETM), *Geochem. Geophys. Geosyst.*, *8*(12), doi:10.1029/2007GC001784.
Rosenbloom, N. A., and R. S. Anderson (1994), Hillslope and channel evolution in a marine terraced landscape, Santa Cruz, California, *J. Geophys. Res.*, *99*(B7), 14,013–14,029, doi:10.1029/94JB00048.
Rowley, D. B., A. M. Forte, R. Moucha, J. X. Mitrovica, N. A. Simmons, and S. P. Grand (2013), Dynamic topography change of the eastern United States since 3 million years ago, *Science*, *340*(6140), 1560–1563, doi:10.1126/science.1229180.
Rudge, J. F., M. E. Shaw Champion, N. White, D. McKenzie, and B. Lovell (2008), A plume model of transient diachronous uplift at the Earth's surface, *Earth Planet. Sci. Lett.*, *267*, 146–160, doi:10.1016/j.epsl.2007.11.040.
Rudge, J. F., G. G. Roberts, N. J. White, and C. N. Richardson (2015), Uplift histories of Africa and Australia from linear inverse modeling of drainage inventories, *J. Geophys. Res. Earth Surf.*, *120*, 894–914, doi:10.1002/2014JF003297.
Saunders, A. D., J. G. Fitton, A. C. Kerr, M. J. Norry, and R. W. Kent (1997), The North Atlantic Igneous Province, in *Geophysical Monograph Series: Large Igneous Provinces: Continental, Oceanic, and Planetary Flood Volcanism*, edited by J. J. Mahoney and M. F. Coffin, 45–93, AGU, Washington, D. C., doi:10.1029/GM100p0045.
Schubert, G., D. L. Turcotte, and P. Olsen (2001), *Mantle Convection in the Earth and Planets*, Cambridge Univ. Press, Cambridge, U. K.
Sclater, J. G., and P. A. F. Christie (1980), Continental stretching: An explanation of the post-mid-Cretaceous subsidence of the central North Sea Basin, *J. Geophys. Res.*, *85*(B7), 3711–3739, doi:10.1029/JB085iB07p03711.
Shaw-Champion, M. E., N. J. White, S. M. Jones, and J. P. B. Lovell (2008), Quantifying transient mantle convective uplift: An example from the Faroe-Shetland basin, *Tectonics*, *27*, doi:10.1029/2007TC002106.
Smith, W. H. F., and D. T. Sandwell (1997), Global seafloor topography from satellite altimetry and ship depth soundings, *Science*, *277*, 1957–1962.
Spice, H. E., J. G. Fitton, and L. A. Kirstein (2016), Temperature fluctuation of the Iceland mantle plume through time, *Geochem. Geophys. Geosyst.*, *17*, 243–254, doi:10.1002/2015GC006059.
Tarboton, D. G. (1997), A new method for the determination of flow directions and upslope areas in digital elevation models, *Water Resour. Res.*, *33*(2), 309–319.
Thomas, J. (1996), The occurrence of the dinoflagellate cyst Apectodinium (Costa & Downie 1976) Lentin & Williams 1977 in the Moray and Montrose Groups (Danian to Thanetian) of the UK central North Sea, *Geol. Soc. Spec. Publ.*, *101*, 115–120, doi:10.1144/GSL.SP.1996.101.01.07.
Thorbergsson, G., I. T. Magnússon, and G. Pálmason (1993), *Gravity Data and Gravity Map of Iceland*, Orkustofnun, Reykjavik, Iceland.
Tiley, R., D. McKenzie, and N. White (2003), The elastic thickness of the British Isles, *J. Geol. Soc. London*, *160*, 499–502.
Underhill, J. R. (2001), Controls on the genesis and prospectivity of Paleogene palaeogeomorphic traps, East Shetland Platform, UK North Sea, *Mar. Pet. Geol.*, *18*(2), 259–281, doi:10.1016/S0264-8172(00)00067-2.
Vandenberghe, N., F. J. Hilgen, R. P. Speijer, J. G. Ogg, F. M. Gradstein, O. Hammer, C. J. Hollis, and J. J. Hooker (2012), The Paleogene period, in *The Geologic Time Scale 2012*, edited by F. M. Gradstein et al., pp. 855–921, Elsevier, Oxford, U. K., doi:10.1016/B978-0-444-59425-9.00028-7.
Vogt, P. R. (1971), Asthenosphere motion recorded by the ocean floor south of Iceland, *Earth Planet. Sci. Lett.*, *13*(1), 153–160, doi:10.1016/0012-821X(71)90118-X.
Wessel, W. H. F., and P. Smith (1990), Gridding with continuous curvature splines in tension, *Geophysics*, *55*(3), 293–305.
Whipple, K. X., and G. E. Tucker (1999), Dynamics of the stream-power river incision model: Implications for height limits of mountain ranges, landscape response timescales, and research needs, *J. Geophys. Res.*, *104*(B8), 17,661–17,674, doi:10.1029/1999JB900120.
White, N. (1990), Does the uniform stretching model work in the North Sea?, in *Tectonic Evolution of the North Sea Rifts*, edited by D. J. Blundell and A. D. Gibbs, pp. 217–239, Oxford Univ. Press, Oxford, U. K.
White, N., and B. Lovell (1997), Measuring the pulse of a plume with the sedimentary record, *Nature*, *4192*, 888–891, doi:10.1038/43151.
White, R., and D. McKenzie (1989), Magmatism at rift zones: The generation of volcanic continental margins and flood basalts, *J. Geophys. Res.*, *94*(B6), 7685–7729, doi:10.1029/JB094iB06p07685.
White, R., and D. McKenzie (1995), Mantle plumes and flood basalts, *J. Geophys. Res.*, *100*(B9), 17,543–17,585.
White, R. S., J. W. Brown, and J. R. Smallwood (1995), The temperature of the Iceland plume and origin of outward-propagating V-shaped ridges, *J. Geol. Soc.*, *152*, 1039–1045, doi:10.1144/GSL.JGS.1995.152.01.26.
Williams, G. L., and J. P. Bujak (1989), Mesozoic and Cenozoic dinoflagellates, in *Plankton Stratigraphy*, edited by H. M. Bolli, J. B. Saunders, and K. Perch-Nielsen, 847–964, Cambridge Univ. Press, Cambridge, U. K.
Wyllie, M. R. J., A. R. Gregory, and L. W. Gardner (1956), Elastic wave velocities in heterogenous and porous media, *Geophysics*, *21*(1), 41–70, doi:10.1190/1.1438217.
Ziegler, P. A. (1992), European Cenozoic rift system, *Tectonophysics*, *208*(1–3), 91–111, doi:10.1016/0040-1951(92)90338-7.